

Prompt: Probability-Conserved Cross Section Biasing Monte Carlo Particle Transport System

Zi-Yi Pan^{a,b}, Ni Yang^{a,b,c}, Ming Tang^{a,b}, Peixun Shen^{a,b}, Xiao-Xiao Cai^{a,b,*}

^a*Institute of High Energy Physics, Chinese Academy of Sciences, China*

^b*Spallation Neutron Source Science Center, China*

^c*University of Chinese Academy of Sciences, China*

Abstract

An open source software package for simulating thermal neutron propagation in geometry is presented. In this system, neutron propagation can be treated by either the particle transport method or the ray-tracing method. Supported by an accurate backend scattering physics engine, this system is capable of reproducing neutron scattering experiments in complex geometries and is expected to be used in the areas of instrument characterisation, optimisation and data analysis.

In this paper, the relevant theories are briefly introduced. The simulation flow and the user input syntax to control it are provided in detail. Five benchmarking simulations, focusing on different aspects of simulation and scattering techniques, are given to demonstrate the applications of this simulation system. They include an idealised total scattering instrument, a monochromatic powder diffractometer, a neutron guide, a chopper and an imaging setup for complex geometries. Simulated results are benchmarked against experimental data or well-established software packages when appropriate. Good agreements are observed.

PROGRAM SUMMARY

Program Title: Prompt

Developer's repository link: <https://gitlab.com/cinema-developers/prompt>

Programming language: C++, C and Python

*Corresponding author: caixx@ihep.ac.cn

External routines/libraries: NCrystal, VecGeom, MCPL, PyVista

Licensing provisions: Apache License, 2.0 (Apache-2.0)

Nature of problem:

It is challenging for traditional neutron ray-tracing simulation methods to consider multiple scatterings in complex geometries, hence the accuracy and precision of the simulated neutron scattering experiments are limited.

Solution method: A hybrid system of Monte Carlo particle transport method and ray-tracing method is proposed.

1. Introduction

Along with the instrument design activities at the powerful neutron spallation sources over the last decades [Tay06, MAA⁺06, KYN⁺19, LBC⁺11, WCC⁺09], Monte Carlo ray-tracing codes emerged as the de facto standard for neutron instrument characterisation and optimisation. There are many packages currently available, such as McStas [LN99], VITESS [ZLM02], and RESTRAX/SIMRES [ŠK97, SK04]. Most of them employ the linear chain method, in which an instrument is decomposed into a series of components and the neutron beam is only allowed to transmit from an upstream component, to the adjoining downstream component. This method is computationally efficient and proven to be highly valuable in estimating neutron instrument flux on the sample [LNA⁺06, CKL⁺18, SDJE06, OMR⁺04] and resolution functions [ASL⁺12, KNI⁺11, EPN⁺11]. A recent review on the state-of-the-art of these packages can be found in [WL20].

There are cases when a neutron stream is split and goes into multiple downstream components. To address these cases, McStas offers a flexible “GROUP” keyword for users to specify the paths. On the other hand, VITESS implements similar approach in several special components, such as the Fermi choppers, supermirrors and crystal analysers [ZLM⁺04]. However, the linear chain method becomes more cumbersome for complex geometries, where the internal structures cannot be arranged in an upstream-downstream manner. For instance, in an assembly of a sample environment vessel containing a sample, the unwanted scatterings from the vessel can occur before or after neutrons passing by the sample. To address this problem, McStas introduced the Union component [Ber17] to allow the definition of complex internal structures. The neutron path within this component depends only on the geometry and scattering physics.

It is worth noting that the linear chain method is not enforced in NISP [DSTH99, SD04], a package developed in the 1990s. This package inherits a part of the Monte Carlo engine from an early version of a particle transport code [WL20]. Due to the absence of the linear assumption, neutrons in this package are not

travelled in a pre-defined chain, hence the simulation is more realistic.

Despite fewer assumptions being made, NISP is not currently among the most popular packages. Apart from the computational efficiency, license and manpower shortage problems outlined in [WL20], a limited number of scattering models in bulk materials could also be a major disadvantage. The departure between the model and actual physics introduces errors in the cross section and leads to inaccurate results. Since 2015, NCrystal [CK20a], a general purpose open-source engine for neutron scattering has been under active development. In this package, microscopic cross sections are calculated based on material basic properties [CKKM19, KC21, KC23]. Thanks to the implemented robust numerical methods, neutron scattering can be modelled in a wide energy range, from ultracold to tens of electronvolts.

The presented software package, probability-conserved cross section biasing Monte Carlo particle transport system (**Prompt**), is our first attempt to tackle the cross section challenge. Available neutron scattering models and the probability-conserved cross section biasing technique are briefly introduced in Section 2. Section 3 explains the concepts of the system along with code examples and shows a minimal but complete simulation input script. Section 4 demonstrates overall system performance by studying a few problems, including an idealised total scattering instrument, a monochromatic powder diffractometer, a neutron guide, an imaging setup for complex geometries and a disk chopper. This work is discussed and concluded in section 5.

2. Theories

The objective of the system is outlined in section 2.1. Section 2.2 and 2.3 introduce the neutron scattering length and scattering types, respectively. As the theory of neutron scattering is given elsewhere in more detail, e.g. [Lov84, Squ12, Sch14], these sections are dedicated to introducing the physical meanings of the relevant parameters and the underneath cross section models. Section 2.4 introduces the implemented probability-conserved cross section biasing method

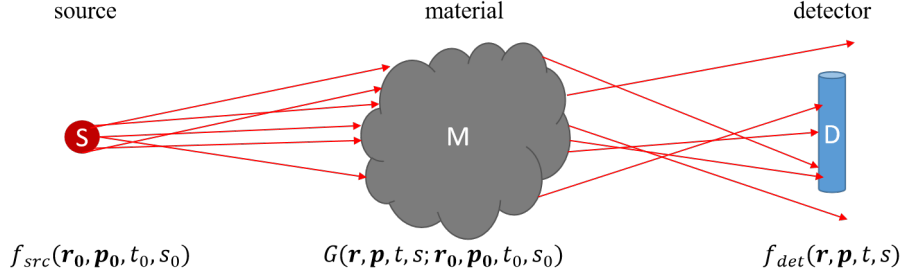


Figure 1: A simplified sketch of particle detection after a volume of material

that is able to effectively control the interaction number of neutrons in a finite volume. Section 2.5 introduces the mirror and chopper models.

2.1. The scope of the system

Fig. 1 illustrates that particles that are originated from the source interact with a volume of material. A part of the particles is detected by a detector at the end. The problem of interest here is the probability of detection, $f_{det}(\mathbf{r}, \mathbf{p}, t, s)$.

From the viewpoint of particle transport, it can be expressed as

$$f_{det}(\mathbf{r}, \mathbf{p}, t, s) = \int d^3\mathbf{r}_0 \int d^3\mathbf{p}_0 \int dt_0 \int ds_0 G(\mathbf{r}, \mathbf{p}, t, s; \mathbf{r}_0, \mathbf{p}_0, t_0, s_0) f_{src}(\mathbf{r}_0, \mathbf{p}_0, t_0, s_0) \quad (1)$$

where \mathbf{r} is the position, \mathbf{p} is the momentum, t is the time, s is the spin, and G function is the propagator.

This high-dimensional integral is typically evaluated using Monte Carlo particle transport systems, in which the propagator is decomposed into geometry and physics modules in general. In such systems, the physics module predicts the particle states by sampling the physical distributions for given prior states, materials and any applied external fields; while the geometry model traces individual particles in volumes along their trajectories.

On the other hand, the ray-tracing method simplifies the integration by a scaling function ϵ , which represents the weight adjustment of the particles. In addition, when the linear chain approximation is applied, the ϵ function is set

to zero if the leaving particles do not intersect with the detector.

$$f_{det}(\mathbf{r}, \mathbf{p}, t, s) = \epsilon(\mathbf{r}, \mathbf{p}, t, s; \mathbf{r}_0, \mathbf{p}_0, t_0, s_0) f_{src}(\mathbf{r}_0, \mathbf{p}_0, t_0, s_0) \quad (2)$$

This method describes neutron transmission behaviour reasonably well in many optical components. One of the simplest examples is the rotating neutron disk chopper. The ϵ function is either unity or zero, representing respectively the event of neutron transmission or absorption.

The objective of `Prompt` is to solve Eq. 1 in bulk materials and Eq. 2 to model moving optical components, i.e. choppers. The linear chain approximation is relaxed in the system. Only thermal neutrons are supported in this version of code. Notice that the gravitational field that may be important when simulating cold neutrons in a long beam guide. By limiting the particle step size, it is possible to simulate the gravitational effects. However, such implementation is computational demanding and outside the scope of current version of the code. It is not yet supported.

2.2. Neutron scattering length

The introduction starts with a limiting case, where neutrons scatter with a stationary nucleus that is fixed at a position throughout the scattering process. If the target nucleus remains in the ground electronic state, and the neutron wavelengths are much longer than the range of neutron-nucleus interaction, the scatterings are contributed only by the s -wave components in terms of partial waves [Sch14]. The scatterings in that case are essentially elastic isotropic and can be characterized by a single parameter b , the so-called *bound* scattering length [Lov84]. The cross section for this hypothetical ¹ case is simply $4\pi|b|^2$.

In the opposite limiting case, where the motion of a nucleus is not hindered at all, the process can be viewed as elastic scattering in the centre of mass frame of reference. The so-called *free* scattering length for this case can be derived [Squ12] to be $b_f = bM/(m + M)$, where m and M are the mass of the

¹Fixing a stationary nucleus is only sound classically, but violates the uncertainty principle.

neutron and target nucleus, respectively. When the incident neutrons are far more energetic than the chemical bonds in the system, say above a few electronvolts, the scattering cross section is approaching the limiting value $4\pi|b_f|^2$, for instance, see ref. [DGM14].

The angular distributions in the laboratory and centre-of-mass frames can be correlated as Eq. 3 [Sch14]. From the viewpoint of this equation, the angular distribution of the *bound* situation is a special case for the *free* situation when γ is approaching zero, i.e. the mass of the target nucleus is infinity in comparison with a neutron.

$$P(\theta_{lab}) = \frac{(1 + \gamma^2 + 2\gamma \cos \theta_{c.m.})^{3/2}}{|1 + \gamma \cos \theta_{c.m.}|} P(\theta_{c.m.})$$

with $\gamma = \frac{m}{M}$ (3)

However, neither the *bound* nor the *free* cases can describe the neutron scattering process adequately accurately in a finite and correlated system, especially when incident neutron wavelengths are comparable with the shortest inter-atomic distances.

Notice that the scattering length b is complex in general. The amplitude of absorption is the imaginary part of b . For thermal neutrons, it is generally adequately accurate to decouple the absorption and scattering processes, see more discussions in section 2.2 of [CKKM19]. As a result, the scattering lengths are typically real-valued for cross section calculations. The absorption cross sections, without considering nuclear resonances, are often taken to be inversely proportional to the neutron velocity, and insensitive to atomic structure and dynamics.

2.3. Neutron scattering cross section

Neutral particles exhibit step-like behaviours in materials. In the Lambert-Beer law, the probability of observing a free particle at length x in a homogeneous material can be described as

$$P(x) = \exp(-\rho\sigma x) \quad (4)$$

where ρ is the scatter number density and σ is the cross section. The cross section can be calculated from the double differential cross section.

$$\sigma = \int \int \frac{d^2\sigma}{d\Omega dE'} d\Omega dE' \quad (5)$$

Under the Born approximation and Fermi's golden rule, the thermal neutron scattering cross section is the double integral of the scattering function scaled by the ratio of the scattered and incident wavenumbers [CK20b],

$$\sigma(\vec{k}_i) = \int \int \frac{|\vec{k}_f|}{|\vec{k}_i|} S(\vec{Q}, \omega) d\Omega dE' \quad (6)$$

with $\vec{Q} = \vec{k}_i - \vec{k}_f$ and $\hbar\omega = \hbar^2(k_i^2 - k_f^2)/2m$, to obey the conservation law of momentum and energy. Here \vec{Q} and ω are the reduced momentum and energy transfers, respectively.

The evaluation and implementation of Eq. 6 depend on the orientation distributions of the statistically equivalent subsystems with respect to the laboratory frame of the simulation system [CK20a, KC21]. For oriented materials, i.e. single and layered crystals, the relevant crystal axes should be aligned with the simulated laboratory frame of reference. So that the moment transfer in the predefined scattering function is identical with that in the simulation world. See more discussions in section 3.5 on how to configure the alignment.

The neutron scattering function can be decomposed into a series of $S_{j,j'}(\vec{Q}, \omega)$, the partial scattering function, contributed by the j_{th} and j'_{th} nuclei pairs [VH54].

$$S(\vec{Q}, \omega) = \sum_{j,j'=1}^N \overline{b_j b_{j'}} S_{j,j'}(\vec{Q}, \omega) \quad (7)$$

Here N is the number of nuclei, $\overline{b_j b_{j'}}$ emphasizes the averaging is performed over the isotopes and spins of all the subsystems.

For a more realistic treatment of the scattering, in the case that the value b for the j_{th} nucleus has no correlation with the isotope and spin, the averaging is

$$\overline{b_j b_{j'}} = \begin{cases} \overline{b_j} \cdot \overline{b_{j'}}, & \text{for } j \neq j' \\ \overline{b_j^2}, & \text{for } j = j' \end{cases} \quad (8)$$

Therefore,

$$\begin{aligned} S(\vec{Q}, \omega) &= \sum_{\substack{j, j'=1 \\ j \neq j'}}^N \overline{b_j} \overline{b_{j'}} S_{j, j'}(\vec{Q}, \omega) + \sum_j^N \overline{b_j^2} S_{j, j}(\vec{Q}, \omega) \\ &= S_{\text{distinct}}(\vec{Q}, \omega) + S_{\text{self}}(\vec{Q}, \omega) \end{aligned} \quad (9)$$

$$= S_{\text{distinct}}(\vec{Q}, \omega) + S_{\text{self}}(\vec{Q}, \omega) \quad (10)$$

In Eq. 10, the first term is originated from the pairs that are built by different nuclei and is known as the *distinct* scattering. The second term is contributed from a single nucleus solely, hence called the *self* scattering.

Inserting $\overline{b^2} = \overline{(b - \bar{b})^2} + (\bar{b})^2$ into Eq. 9, one can obtain

$$\begin{aligned} S(\vec{Q}, \omega) &= \sum_{j, j'=1}^N \overline{b_j} \overline{b_{j'}} S_{j, j'}(\vec{Q}, \omega) + \sum_j^N [\overline{b_j^2} - (\bar{b}_j)^2] S_{j, j}(\vec{Q}, \omega) \\ &= S_{\text{coh}}(\vec{Q}, \omega) + S_{\text{inc}}(\vec{Q}, \omega) \end{aligned} \quad (11)$$

$$= S_{\text{coh}}(\vec{Q}, \omega) + S_{\text{inc}}(\vec{Q}, \omega) \quad (12)$$

where S_{coh} and S_{inc} are the coherent and incoherent scatterings, respectively. Coherent scattering can be physically interpreted as the scattering that would arise if all the scattering lengths equal to their mean value. While the incoherent scattering, proportional to the self scattering, represents the deviations of the scattering lengths from their mean value. It is worth emphasising that the coherent scattering is contributed by distinct scattering as well as a part of the self scattering.

$$S_{\text{coh}}(\vec{Q}, \omega) = S_{\text{distinct}}(\vec{Q}, \omega) + \sum_j^N \overline{b_j^2} S_{j, j}(\vec{Q}, \omega) \quad (13)$$

Coherent and incoherent scatterings can be further categorised by whether the neutron exchanges energy with the system, i.e. elastic and inelastic with respect to the laboratory frame of reference.

$$S(\vec{Q}, \omega) = S_{\text{coh}}^{\text{el}}(\vec{Q}, \omega) + S_{\text{coh}}^{\text{inel}}(\vec{Q}, \omega) + S_{\text{inc}}^{\text{el}}(\vec{Q}, \omega) + S_{\text{inc}}^{\text{inel}}(\vec{Q}, \omega) \quad (14)$$

2.3.1. Elastic scattering

Homogeneous liquids and gases do not exhibit elastic scattering [Squ12, Cre13]². In the backend scattering engine, elastic scatterings are originated explicitly from solid type materials.

The scattering functions of the incoherent and coherent elastic scattering are shown in Eq. 15 and 16, respectively.

$$S_{\text{inc}}^{\text{el}}(\vec{Q}, \omega) = N \sum_j^N [\overline{b_j^2} - (\overline{b_j})^2] \exp(-2W_j) \quad (15)$$

$$S_{\text{coh}}^{\text{el}}(\vec{Q}, \omega) = N \frac{(2\pi)^3}{v_0} \sum_{\vec{\tau}} \delta(\vec{Q} - \vec{\tau}) \left| \sum_j^N \overline{b_j} \exp(i\vec{Q} \cdot \vec{R}_j) \exp(-W_j) \right|^2 \quad (16)$$

W is the Debye-Waller factor, v_0 is the unit cell volume, $\vec{\tau}$ is the lattice point in the reciprocal space, and \vec{R} is the equilibrium position.

For idealised materials, the orientations of crystal unit cells are described by distribution functions. Numerical procedures are implemented to compute the effective scattering functions averaged over the given distribution. The averaging is rather sophisticated and outside the scope of this paper, refer to Ref. [KC21] for the detailed methods. The backend scattering engine supports the elastic scatterings in isotropic powders, mosaic single crystals and mosaic layer crystals.

²Indeed, measuring these materials in an elastic type neutron instrument does produce event data. However, this type of instrument generally guarantees that the event data are analysed without considering energy exchange in scatterings, but not what the actual physical processes are taking places.

2.3.2. Inelastic scattering

Limited by the memory footprint and initialisation time of typical Monte Carlo simulations, inelastic scattering is only supported in isotropic materials, e.g. powder and liquid.

It has been shown that the incoherent part of the inelastic scattering for ideal crystal powders in the harmonic approximation [Sjö58] and liquids in the Gaussian approximation under the fluctuation-dissipation theorem [RSS62] can arrive independently to the identical form,

$$S_{\text{inc}}^{\text{inel}}(Q, \omega) = \frac{1}{2\pi} \int e^{-i\omega t} \exp \left[-\frac{Q^2}{2} \Gamma(t) \right] dt \quad (17)$$

Here the scattering function depends on the modulus of \vec{Q} due to the isotropic nature of the material, and $\Gamma(t)$ is width function.

$$\Gamma(t) = \frac{\hbar}{M} \int_0^\infty d\omega \frac{\rho(\omega)}{\omega} \left[\coth \left(\frac{\hbar\omega}{2k_B T} \right) (1 - \cos \omega t) - i \sin \omega t \right] \quad (18)$$

where $\rho(\omega)$ is the density of states, k_B is the Boltzmann constant and T is the temperature. The expressions indicate that it is adequate to calculate the incoherent cross section in isotropic materials using only the density of states.

The numerical evaluation of Eq. 17 for crystals is computationally efficient when applying the phonon expansion method [Sjö58], therefore it is suitable to evaluate on-the-fly. On the other hand, for liquids, Γ becomes divergent when ω approaches zero, because of the diffusive motions. The scattering function, in that case, is typically pre-computed based on model-assisted evaluation methods [DGM14] or more expansive direct convolutions [DC22].

The coherent inelastic scattering function may also be included in the pre-computed input cross section. In the case of liquid, the Sköld approximation [Skö67], i.e. Eq. 19, is often applied.

$$S_{\text{coh}}^{\text{inel}}(Q, \omega) = \sum_{jj'=1}^N \overline{b_j b_{j'}} S_{jj'}(Q) S_{jj} \left(\frac{Q}{\sqrt{S_{jj'}(Q)}}, \omega \right) \quad (19)$$

$S_{jj'}(Q)$ is the partial static structure factor and equals to $\int S_{jj'}(Q, \omega) d\omega$. As

suggested by the zeroth order sum rule of the scattering functions, it is unity when $j = j'$, i.e. the case of self scattering function.

For numerical simplification, the isotropic incoherent approximation, or otherwise known as the Gaussian approximation [RSS62], is often employed to skip the computation of the coherent inelastic scattering function. In that case, the distinct scattering functions are vanished, hence the overall inelastic scattering is approximated entirely by the inelastic part of the self scattering function (see Eq. 10). The absence of distinct scattering results in a smoothed inelastic scattering function with respect to Q . Consequently, the calculated angular distributions are not expected to be directly comparable with those from measurements in every detail. Nonetheless, in practice, the incoherent approximation is known to be highly useful when the angular distribution is less of concern, in the sense that the final results of interest are the averaged values in a large angular range, such as when measuring phonon density of states (see section 9.16 of [Sch14]), characterising neutron moderation processes [DGM14] and estimating the intensities of multi-phonon scattering background (see the section 3.10 of [Squ12]).

In addition to the incoherent approximation, a Debye model can be used for crystals, when only the structural information is mainly concerned, e.g. powder diffraction of a strong coherent sample. The density of states in that case is proportional to the power of phonon energy and the upper cut-off is defined by the Debye temperature [SSP95].

In the situations where the correlations of the systems are relatively insignificant, e.g. in strong absorbing or gaseous materials, the short-collision-time approximation [MK10, CKKM19], can be used to describe the scattering processes, see section 3.5 for more discussions.

2.4. The cross section biasing mechanism

According to the probability expressed in Eq. 4, the step length of a free particle can be sampled according to

$$l = -\frac{\log_e(\xi)}{\rho\sigma} \quad (20)$$

where ξ is a number generated in a uniform distribution $[0, 1)$.

If an arbitrary positive scaling factor g is applied to the cross section to form an artificial cross section $\sigma_g = g\sigma(E)$, the sampled step length becomes

$$l_g = -\frac{\log_e(\xi)}{g\rho\sigma} \quad (21)$$

In comparison with l , l_g is increased or decreased, when the factor is smaller or greater than unity, respectively. That may effectively control the particle interaction number in a finite volume.

However, altering such an important parameter distorts the step length distribution in Eq. 4 and produces wrong statistical results.

It can be seen that by differentiating Eq. 4, and then dividing the result by $P(x)$, one can obtain

$$\frac{dP(x)}{P(x)} = -\rho(x)\sigma dx \quad (22)$$

When applying an artificial cross section, this equation becomes

$$\frac{dP_g(x)}{P_g(x)} = -\rho(x)\sigma_g dx \quad (23)$$

By the quotient rule of derivative, the impact of applying a biasing factor to the probability along the path can be quantified as

$$\frac{dP_g(x)/P(x)}{dP_g(x)/P(x)} = -(g-1)\rho(x)\sigma dx \quad (24)$$

It has been shown [MW12] that the distribution distortion can be eliminated when the particle weight is corrected by a compensation factor at the end of each interaction as

$$W_n = W_0 \prod_{l=1}^n \frac{1}{g_{m,l}} \prod_{m=1}^n \prod_{i=1}^{N_p} \exp[(g_{m,i} - 1)x_m \rho \sigma_i] \quad (25)$$

Here, W_o is the original weight of the particle; n is the number of interactions, the step length of the m_{th} step is x_m , N_p is the number of reaction processes, the biasing factor for the i_{th} process at the m_{th} step is $g_{m,i}$, the l_{th} process occurs at the end of the m_{th} step, and the corresponding biasing factor is $b_{m,l}$.

The initial aim of the implementation is to facilitate the study of scatterings between an incident neutron beam and a small sample of a scattering instrument. In such a scenario, multiple scatterings are often considered to be a type of weak but important noise. Applying a biasing factor greater than unity, not only the statistics of the single scattering signal can be improved, but also the variances of the multiple scattering noises can be significantly reduced. Detailed validation and performance of this method are discussed in section 4.1 and 4.4.

2.5. Neutron mirror and disk chopper

The empirical reflectivity model in McStas [WFK+22] is used for neutron mirrors. The reflection probability is a piecewise function,

$$R(Q) = \begin{cases} R_0, & \text{if } Q \leq Q_c \\ \frac{1}{2}R_0[1 - \alpha(Q - Q_c)] \left[1 - \tanh\left(\frac{Q - mQ_c}{W}\right) \right], & \text{if } Q > Q_c \end{cases} \quad (26)$$

where R_0 is the low-angle reflectivity, Q_c is the critical scattering wavenumber, α is the reflectivity slope, m is the m-value of the mirror, and W is the cut-off width. The default values retaken from McStas are given in Table 1.

When a neutron is reflected, its energy remains unchanged, so Q only depends on the reflection angle. The reflected direction, \vec{n}_f , can be calculated using the neutron direction \vec{n}_i , and the normal of the contact point \vec{n}_r as

$$\vec{n}_f = \vec{n}_i - 2\vec{n}_r(\vec{n}_i \cdot \vec{n}_r) \quad (27)$$

The neutron disk chopper is a neutron optics component that is modelled in ray-tracing method. The neutron weight is modified by the ray-tracing process instead of detailed scattering and propagation in the transport mode.

Table 1: The parameters of the neutron mirror model and their values retaken from Mcstas `Guide` component. The m -value of mirror is required, while the others are fixed.

Parameter	Value	Description	Unit
m		Mirror m -value	1
R_0	0.99	Low-angle reflectivity	1
Q_c	0.0219	Critical scattering wavenumber	\AA^{-1}
α	6.07	Slope of reflectivity	\AA
W	0.003	Width of cut-off	\AA^{-1}

Table 2: Options of the `Prompt` launcher. Parameters without default values are required, the others are optional.

Option	Default	Description
<code>-g [file]</code>		Set GDML input file.
<code>-s [seed]</code>	4096	Set the seed for the random generator.
<code>-n [number]</code>	100	Set the number of primary events.
<code>-v</code>		The flag to activate the visualisation of geometries and trajectories.

When a neutron arrives at the disk chopper, the ray-tracing method is used. The corresponding ϵ function in Eq. 2 is a mask of position and time. It is unity if a neutron hits a opening window, and is zero otherwise. In the implementation, the disk chopper is considered to be infinitely thin.

3. The program

The executable, `prompt`, reads user input files in the Geometry Description Markup Language (GDML) format [CMPS06] and launches the simulation. The language schema is introduced in the manual of the standard in detail [gdm22]. The available options are summarized in Table 2.

In a typical simulation, statistical distributions of particle histories are iteratively accumulated in a Monte Carlo loop of events. Each event begins with the generation of the particle, and ends with the absorption of the particle in materials or escape of the particle from all the volume boundaries. The accumulators are referred to as scorers in this system and are realised by histograms

that are attached to volumes. The accumulation processes are triggered by the concept of particle tracing states (PTS) on the volume.

The simulation flow is illustrated in section 3.1. Available particle generators, i.e. particle guns, are presented in section 3.2. The volume and scorers are introduced in section 3.3 and 3.4, respectively. The syntax for initialising physics models is described in section 3.5. Finally, a short example of input script is listed and explained in section 3.6.

3.1. Simulation flow

The flow of the simulation is divided into two phases, the tracing phase and the interaction phase, as illustrated in Fig. 2.

The system first looks for the volume that contains the last particle in the particle stack. The successful determination of a valid volume indicates that the particle is inside the world, i.e. the largest volume that contains all the child volumes in the simulation. Otherwise the simulation for this particle is terminated. The program then asserts the particle alive status before picking the simulation mode for the interaction phase. If the particle is not just generated at a random position by a particle gun, it must arrive at the boundary of a volume at this stage. In that case, the system checks whether a ray-tracing model is defined for the volume, before branching out into the ray-tracing mode or the transport mode.

In the transport mode, the particle is first treated by the mirror, if it is specified. Next, the macroscopic total cross section is evaluated, and the step length is sampled using Eq. 21. If the sampled step is longer than the maximum distance that allowed by the volume, the particle is moved to the geometry intersection point and enters the relocation subprocess. Otherwise, the particle is moved forward to the location where an interaction takes place. In this case, the particle enters the propagation subprocess or the absorption subprocess, depending on the sampling on the cross sections. In any case, whenever the particle is moved, the weight is adjusted according to Eq. 25, if the cross section is biased.

In the ray-tracing mode, the particle is simulated in Eq. 2. The main difference between this mode and the transport mode are that the particle states in the volume is completely manipulated by the implemented model. The system views the ray-tracing volume as a black box and has no knowledge about the particle states, until the model decides to eliminate the particle or sends the particle to the boundary of the volume. Notice that, a volume containing child volumes is not supported by the ray-tracing mode, as the internal structure of the volume can not be modelled systematically.

The sub-routines of the interaction phase are presented in Fig. 3. They can modify particle parameters such as location, energy and direction of motion, as well as changing the particle tracing states that can trigger available scorers. More details of the scorers are introduced in section 3.4.

In the relocation sub-routine shown in Fig. 3a, the particle is moved to the boundary of the next volume, with the momentum unchanged. In the propagation sub-routine shown in Fig. 3b, the scattering angle and energy of the particle are sampled. In the absorption sub-routine shown in Fig. 3c, the alive status of the particle is set to false.

3.2. Particle gun

The initial neutron position, momentum direction, energy and time are generated by particle guns. A few types of guns are initially provided in this version of `Prompt` to facilitate the modelling of point sources, surface sources and particle histories in the standard Monte Carlo Particle Lists (MCPL) format from other software packages.

Two basic particle guns, which can create neutron point sources, are provided, namely, `SimpleThermalGun` and `IsotropicGun`. There are three ways to specify neutron energies in these two guns, using a single value, sampling from uniform distribution or a Maxwell–Boltzmann distribution of coefficient kT . The `SimpleThermalGun` can produce neutrons aiming in a single direction, as shown in Listing 1. While the `IsotropicGun` can produce isotropic neutrons, in which the momentum direction is equiprobable in all solid angles, see Listing 2.

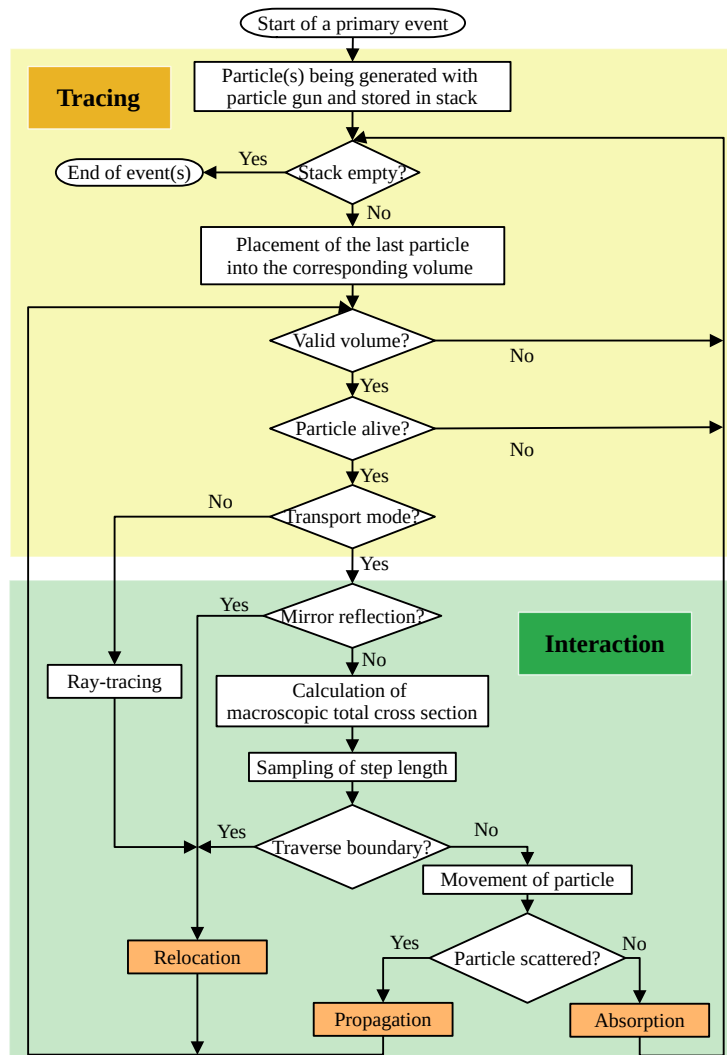


Figure 2: The main simulation flow of a primary event adopted in Prompt

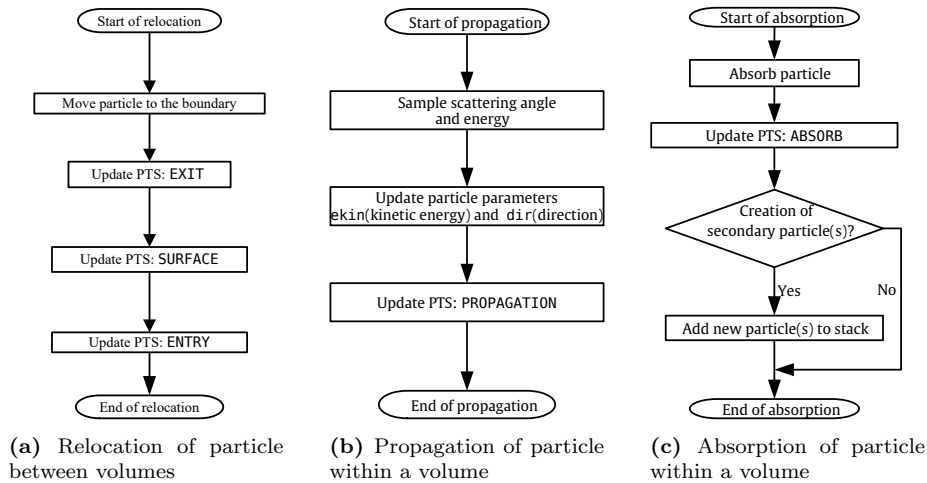


Figure 3: Three types of sub-routines: relocation, propagation and absorption

```
<userinfo>
  <auxiliary auxtype="PrimaryGun" auxvalue="gun=SimpleThermalGun; energy=0.0253;
    position=0,0,0; direction=1,0,0" />
</userinfo>
```

Listing 1: SimpleThermalGun that produces neutrons with energy of 0.0253 eV, position of (0, 0, 0) and direction along x axis.

```
<userinfo>
  <auxiliary auxtype="PrimaryGun" auxvalue="gun=IsotropicGun; energy=0.0253;
    position=0,0,0" />
</userinfo>
```

Listing 2: IsotropicGun that produces radial neutron beams with energy of 0.0253 eV, position of (0, 0, 0).

Inspired by McStas, Prompt also provides `UniModeratorGun` and `MaxwellianGun` to generate neutrons from a moderator surface. The particle positions are sampled randomly from a rectangular surface representing a moderator surface. The direction of each is determined by sampling another point in another opening representing a slit as the entrance of neutrons to a beam channel.

The `UniModeratorGun` samples randomly the kinetic energy of neutrons from the uniform distribution formed by the wavelength and the range of wavelength taken as inputs, as shown in Listing 3.

The `MaxwellianGun` takes a temperature as input, and samples randomly the kinetic energy of neutrons from a corresponding Maxwell–Boltzmann distri-

bution, as presented in Listing 4.

```
<userinfo>
  <auxiliary auxtype="PrimaryGun" auxvalue="gun=UniModeratorGun; mean_wl=3.39;
    range_wl=0.3; src_w=100; src_h=50; src_z=-400; slit_w=5; slit_h=10;
    slit_z=1" />
</userinfo>
```

Listing 3: A `UniModeratorGun`, producing neutrons with energy randomly selected between 3.09 Å and 3.69 Å, with position randomly selected in an opening of 100 mm×50 mm located at (0,0,-400) (in mm), with directions determined by connecting two points of two openings

```
<userinfo>
  <auxiliary auxtype="PrimaryGun" auxvalue="gun=MaxwellianGun; src_w=100;
    src_h=50; src_z=-400; slit_w=5; slit_h=10; slit_z=1; temperature=293.15;
    " />
</userinfo>
```

Listing 4: A `MaxwellianGun`, producing neutrons with energy randomly selected ($T = 293.15\text{K}$), with position randomly selected in an opening of 100 mm×50 mm located at (0,0,-400) (in mm), with directions determined by connecting two points of two openings

An example of using an `MCPLGun` is shown in Listing 5. The input files are typically generated by Monte Carlo packages, e.g. McStas, Geant4, MCNP and PHITS. Notice that when preparing the input files, particles other than neutrons have to be filtered out. That can be easily done by using `mcpltool` in the MCPL toolkit as `mcpltool --extract -p2112 example.mcpl justneutrons.mcpl`

```
<userinfo>
  <auxiliary auxtype="PrimaryGun" auxvalue="gun=MCPLGun;
    mcplfile=justneutrons.mcpl" />
</userinfo>
```

Listing 5: A `MCPLGun` reads neutron histories from the specified MCPL files

3.3. Geometry

Prompt uses `VecGeom` [A⁺05] v1.2.0 as the geometry engine and `GDML` [CMPS06] as the language to define the geometry of a simulation. A geometry is a hierarchy of volumes, each of which a shape and a composition should be assigned to. There are three essential parts to describe a volume, namely `solids` for the shape description, `structure` for the hierarchy relationship and `material` for the composition. In this section, the methods to define the `solids` and `structure` are given, and leaving the `materials` part in section 3.5.

The `solids` currently supported in Prompt are retaken from the GDML user's guide [gdm22] and presented in Appendix A. A `solid` defines solid type and the

corresponding parameters. As an example, the lines presented in Listing 6 define a box of the identical length each side. The length unit, `lunit`, is millimeter by default. It can be otherwise chosen to be nanometer (`nm`), micrometer (`um`), centimeter (`cm`), meter (`m`) or kilometer (`km`). The default unit for angle, `ainit`, is degree (`deg`), and radian (`rad`) can also be used, alternatively.

```
<solids>
  <box lunit="mm" name="Cube" x="10.0" y="10.0" z="10.0" />
</solids>
```

Listing 6: A box named *Cube* of 10 mm for each side length

The `structure` is a hierarchy of volumes. A volume is called logical when it refers to a `solid` and a `material`. A logical volume becomes physical when it is positioned into a mother logical volume. Notice that any boundary of a daughter volume should be contained within its mother volume and boundary overlap test is not implemented in this version of the system. All volumes in a simulation are physical because they have to be positioned, except for the `world`, the largest volume on the top of the hierarchy. An example is presented in Listing 7, where a hierarchy of two levels is defined. The first level corresponds to the `world` of this simulation, while the second is a volume named `phy_2ndLevel` placed in the center of the `world`.

```
<solids>
  <box lunit="mm" name="solWorld" x="10" y="10" z="10" />
  <orb lunit="mm" name="solSphere" r="5" />
</solids>
<structure>
  <volume name="2ndLevel">
    <solidref ref="solSphere" />
    <materialref ... />
  </volume>
  <volume name="World">
    <solidref ref="solWorld"/>
    <materialref ... />
    <physvol name="phy_2ndLevel">
      <volumeref ref="2ndLevel" />
      <position name="Position" unit="mm" x="0" y="0" z="0" />
    </physvol>
  </volume>
</structure>
```

Listing 7: A hierarchy of two levels

Table 3: Particle scorers in a volume. The statistical information is presented in form of one-dimensional histogram, if not otherwise noted.

Scorer	Statistical Information
ESpectrum	Energy Spectrum
WlSpectrum	Wavelength spectrum
TOF	Time-of-flight spectrum of particles.
PSD	Two-dimensional spatial spectrum on the projection of a volume
MultiScat	Scattering number spectrum of scattered in a volume
DeltaMomentum	Momentum transfer spectrum
Angular	Angular spectrum
VolFluence	Particle flux spectrum in a volume

3.4. Scorer

Eight scorers that are designed to accumulate particle statistical information in histograms are listed in Table 3. The variables of interest are generally fixed to one of the attributes of the particles, such as energy, position, and time. For a `DeltaMomentum` scorer, the method used to calculate the variable should be chosen from elastic or inelastic scatterings. In the elastic case, the momentum transfer Q is calculated as

$$Q = 2k_i \sin \theta \quad (28)$$

While in the inelastic case, the momentum transfer is

$$Q^2 = k_i^2 + k_f^2 - 2k_i k_f \cos 2\theta \quad (29)$$

To set up, a scorer is attached to a volume from which the statistical information is expected to be extracted. For instance, in Listing 8, a PSD scorer is attached to the volume named `Detector`. The parameters of scorers are listed in Appendix C.

```
<volume name="Detector">
  <materialref ref="Vacuum"/>
  <solidref ref="DetectorSolid"/>
  <auxiliary auxtype="Scorer" auxvalue= "Scorer=PSD; name=NeutronHistMap;
    xmin=-250; xmax=250; numBins_x=100; ymin=-250; ymax=250; numBins_y=100;
    ptstate=SURFACE; type=XY"/>
</volume>
```

Listing 8: A PSD scorer attached to the volume named `Detector`

The `ptstate` in Listing 8 denotes the particle tracing state. The particle tracing states reflect the relationships between the particles and volumes, and also act as triggers allowing scorers to accumulate particle weights. Each scorer should be assigned to a particle tracing state to listen to. In **Prompt** five particle tracing states are defined, as follows:

- **SURFACE**: A particle reaches the geometry boundary of a volume,
- **ENTRY**: A particle enters a volume,
- **ABSORB**: A particle is absorbed in a volume,
- **PROPAGATE**: A particle propagates in a volume,
- **EXIT**: A particle exits a volume.

All of them are available for all scorers, except that `MultiScat` is immutably set to `PROPAGATE`.

To illustrate the triggering mechanism of scorers, the transport process of a particle in the geometry of Listing 7 is shown in Fig. 4. The particle transports four steps in this simple geometry. In step 1, when the particle reaches point A at the boundary of volume Sphere, it simultaneously exits volume World and enters volume Sphere. Therefore, it can trigger the scorer that is listening to the `EXIT PTS` of the volume World and the `SURFACE` and `ENTRY PTS` of the volume Sphere. In step 2, when the particle arrives at point B, it is possible to trigger the `PROPAGATE` or `ABSORB PTS` of the volume Sphere. In this example, it is chosen to be `PROPAGATE` so that the simulation continues. Similar to step 1, when the particle reaches point C at the end of step 3, it can trigger the scorer on volume Sphere set to `EXIT` and the scorer on volume World set to `ENTRY`. When the particle reaches point D at the end of step 4, it is at the boundary of volume World and will be out of volume World. Hence, it is killed and can trigger the scorer on volume World set to `EXIT`.

It is worth noting that the `SURFACE` and `ENTRY` can be used interchangeably for scorers. These two PTS are used in the core of the system to indicate whether the interaction is treated using the surface or bulk material models.

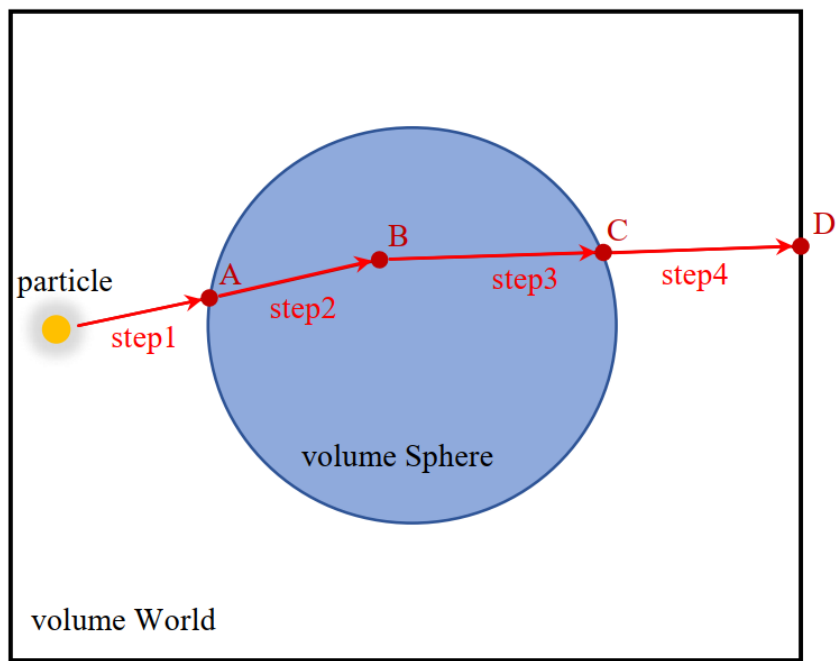


Figure 4: Transport process of a particle in a simple geometry

A scorer creates one or several histograms showing the statistical results. They are encoded in the `Numpy` array format [HMvdWea20] which are then stored in the header of output MCPL [KKK⁺17] files. In addition, a Python script is generated along with each MCPL file to show the basic read and plot functions for post-analysis.

3.5. Simulation physics

`Prompt` defines three types of physics, namely, bulk material physics, mirror physics and ray-tracing physics.

All bulk material cross sections are computed by the backend engine `NCrystal` v3.0.0. The syntax for defining an ideal isotropic Al polycrystal is shown in Listing 9. The physics configuration string that is passed to `NCrystal` for the calculation of averaged cross section per atom is enclosed in single quotation marks. The configuration string syntax and basic crystal parameters in the `.ncmat` file are explained in the reference paper [CKKM19] and the official Wikipedia [KC23] of `NCrystal` in detail. In this example, the cross section biasing factors for both the scattering and absorption models are doubled. Notice that in the special case, where a factor is set to zero, the corresponding model is removed from the simulation.

```
<material name="Al_biased">
  <atom value="physics=ncrystal;nccfg='Al_sg225.ncmat';
              scatter_bias=2.0;abs_bias=2.0"/>
</material>
```

Listing 9: Example of defining an ideal Al polycrystal material with user specified cross section biasing factors

The biasing factors are unity by default. Indicated by Eq. 25, which effectively disables the cross section biasing mechanism. Equivalently, the material definition can be simplified by only passing the `NCrystal` physics configuration string, as Listing 10.

```
<material name="Al">
  <atom value="Al_sg225.ncmat"/>
</material>
```

Listing 10: Defining the same material as Listing 9 but with unity cross section biasing factors

For oriented isotropic Gaussian mosaic single crystals, in order to unambiguously define the unit cell orientations, two non-parallel vectors in the Miller indices and their corresponding laboratory directions should be specified [CK20a]. For example, the definition of Ge-511 monochromator is followed.

```
<material name="Ge">
  <atom value="Ge_sg227.ncmat;mos=0.3deg;
    dir1=@crys_hkl:5,1,1@lab:0,0,1;
    dir2=@crys_hkl:0,1,-1@lab:1,0,0"/>
</material>
```

Listing 11: Ge-511 single crystal with 0.3° isotropic Gaussian mosaicity

For layered crystals, i.e. crystals consisting of parallel layers, additional `lcaxis`, the averaged normal of the layers should be specified [KC21] as showing in the Listing 12. Notice that, repetition of the `lcaxis` in the configuration string is not required, if it is already embedded in the `.ncmat` input file.

```
<material name="Graphite">
  <atom value="C_sg194_pyrolytic_graphite.ncmat;mos=2deg;
    dir1=@crys_hkl:0,0,2@lab:0,0,1;
    dir2=@crys_hkl:1,0,0@lab:1,0,0;
    lcaxis=0,0,1"/>
</material>
```

Listing 12: Pyrolytic graphite-002 layered crystal with 2° mosaicity

The backend engine also supports the so-called “unstructured materials” [KC23], *freegas::* and *solid::*. They are well-suited to describe gaseous or strong absorbing materials in which atomic scale configurations contribute insignificantly to the total cross section. The *freegas::* type materials use the classical two-body collision model to treat the scattering, while the *solid::* type material models apply the phonon expansion method using the Debye density of states to prepare the inelastic scattering function. For the later material type, additional incoherent elastic scatterings are also included.

```
<material name="Air">
  <atom value="freegas::N78O22/1.225kgm3"/>
</material>
<material name="enriched_B4C">
  <atom value="solid::B4C/2.5gcm3/B_is_0.95_B10_0.05_B11"/>
</material>
```

Listing 13: Examples of defining dry air with 78% N and 22% O and enriched B_4C solid with 95% ^{10}B and 5% ^{11}B

The mirror model is implemented as a surface process. It should be attached to a given volume to describe the specular reflection. A mirror can be specified

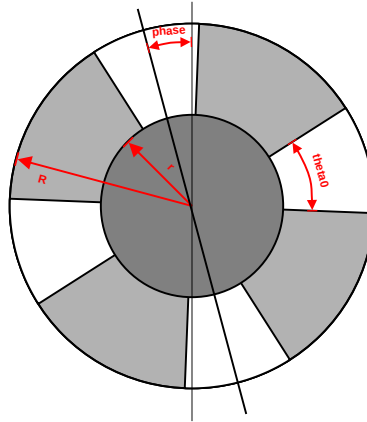


Figure 5: An illustration of the DiskChopper with $n = 4$ opening windows in Prompt, with `phase` the angle deviated from the origin (position at time zero), `theta0` the opening angle of each window, `r` the inner radius, `R` the outer radius (which is the radius of the tube to which the DiskChopper is attached).

by associate a `SurfaceProcess` to a volume. An example is given in Listing 14. See more discussions on surface type physics at the end of section 3.4.

```
<volume name="lv_Mirror">
  <solidref ref="solid_mirror"/>
  <materialref ref="Si"/>
  <auxiliary auxtype="BoundaryPhysics" auxvalue="physics=MirrorPhysics;m=2.0"/>
</volume>
```

Listing 14: Examples of defining a mirror with $m=2$, see Eq. 26

A DiskChopper of Prompt is a ray-tracing physics similar to the DiskChopper component of McStas. An example is provided in Listing 15, which adds a DiskChopper to the simulation. The parameters are listed in Table. 4. The geometry of the disk is illustrated in Fig. 5. The central circular area of radius r is completely black to neutrons. There are $n = 4$ periodic opening windows that are evenly distributed in 2π . The angle of a window is defined by θ_0 . The positive rotational frequency indicates the rotational direction that follows the right-hand rule.

```
<solids>
  <tube lunit="mm" name="solid_DiskChopper" rmin="0.0" rmax="250.0" z="0.001"
    deltaphi="360.0" startphi="0.0"/>
</solids>
<structure>
  <volume name="lv_DiskChopper">
    <solidref ref="solid_DiskChopper" />
  </volume>
</structure>
```

Table 4: The parameters of DiskChopper. All of the parameters are required.

Parameter	Description	Unit
r	Inner radius of the disk chopper	mm
n	Number of window. If multiple windows are defined, they are evenly arranged in 2π .	1
rotFreq	Rotation frequency.	Hz
theta0	Opening angle of each window.	°
phase	Angle deviated from the position at time zero.	°

```
<materialref ref="Vacuum" />
<auxiliary auxctype="SurfaceProcess" auxvalue="physics=DiskChopper;
  rotFreq=100; r=130; theta0=20; n=4; phase=0"/>
</volume>
</structure>
```

Listing 15: Examples of defining a disc chopper like Fig. 5

3.6. A minimal example

An example, minimized but involving most of the introduced elements is presented. As a first step, an input is prepared in GDML format, named `example.gdml`, as shown in Listing 16. In this example, the Debye-Scherrer cones of 2.2 \AA incident neutrons from an Al powder sample are measured by a position sensitive detector.

Fig. 6a is the visualisation of one thousand neutron trajectories. It can be reproduced by the command

```
#!/bin/bash
prompt -g example.gdml -v -n 1000
```

A production run can be executed without the visualiser as

```
#!/bin/bash
prompt -g example.gdml -n 5e6
```

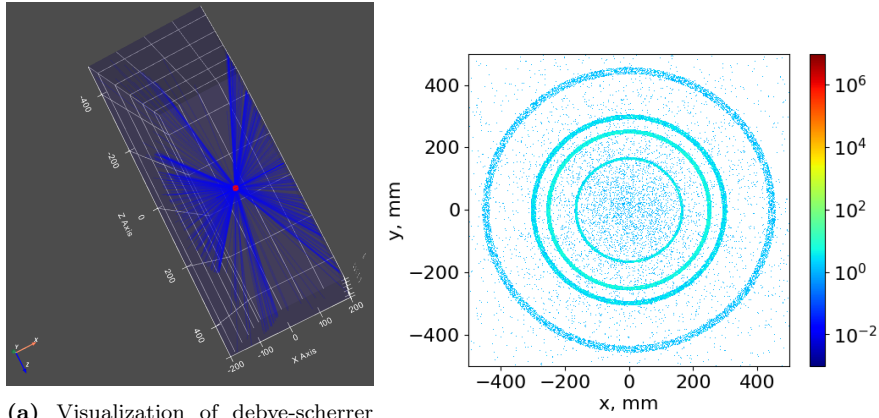
After the simulation, the heatmap of the detector and the corresponding python script template is generated. The heatmap, as shown in Fig. 6b, of the position sensitive score in logarithmic scale can be visualised by running

```
#!/bin/bash
python ScorerPSD_NeutronHistMap_view.py -l
```

It should be noted that the file name of the Python script created depends on the configuration of the scorer.

```
<gdml>
  <userinfo>
    <!-- Defining gun -->
    <auxiliary auxtype="PrimaryGun" auxvalue="gun=SimpleThermalGun;
      energy=0.0169; position=-80.,0.,0.; direction=1,0,0" />
  </userinfo>
  <materials>
    <!-- Defining material -->
    <material name="Universe">
      <atom value="freegas::H1/1e-26kgm3"/>
    </material>
    <material name="Al">
      <atom value="Al_sg225.ncmat"/>
    </material>
  </materials>
  <solids>
    <!-- Defining solid -->
    <box lunit="mm" name="WorldSolid" x="400.0" y="1000.0" z="1000.0" />
    <box lunit="mm" name="SampleSolid" x="10.0" y="10.0" z="10.0" />
  </solids>
  <structure>
    <!-- Defining geometry tree and hierarchy of volumes -->
    <volume name="VolSample">
      <solidref ref="SampleSolid" />
      <materialref ref="Al" />
    </volume>
    <volume name="VolWorld">
      <solidref ref="WorldSolid" />
      <materialref ref="Universe" />
      <!-- Defining PSD scorer and attaching it to World -->
      <auxiliary auxtype="Scorer" auxvalue="Scorer=PSD;
        name=NeutronHistMap; xmin=-500; xmax=500; numBins_x=1000;
        ymin=-500; ymax=500; numBins_y=1000; ptstate=EXIT; type=YZ"/>
      <physvol name="PhysVol_Sample">
        <volumeref ref="VolSample" />
      </physvol>
    </volume>
  </structure>
  <setup name="Default" version="1.0">
    <world ref="VolWorld" />
  </setup>
</gdml>
```

Listing 16: A minimum example of input script in Prompt, example.gdml



(a) Visualization of debye-scherrer cone reproduced by using `Prompt`, (b) Neutrons captured by PSD scorer, Debye-Scherrer cones manifested with four circles with Al powder

Figure 6: Visualization and scoring results of the simulation mission

4. Application and Benchmark

In section 4.1, the total scattering technique is applied to a heavy water sample to investigate the effectiveness of the cross section biasing technique for multiple scatterings. A minimal static source powder diffractometer, including a single crystal monochromator, pattern is simulated in section 4.2. Section 4.3 introduces the simulation of a squared neutron guide as a function of incident wavelength. A complex geometry is in section 4.4 to discuss the impact of the geometry on the overall computational speed. A moving optical component, disk chopper, is presented in section 4.5, showing the capability in ray-tracing process simulation.

4.1. Total scattering

A heavy water sample that is surrounded in a perfect spherical detector is simulated. Fig. 7 shows the visualisation of the geometry and 100 neutron trajectories. In the simulation, a `SimpleThermalGun` is used to emit neutrons in the positive z-axis direction at 3.635 eV. At 10 m downstream of the gun, a 12 mm radius spherical sample is located in the center of the detector, of which the inner radius is 2000 mm and the thickness is 1 mm. A `MultiScat` scorer is

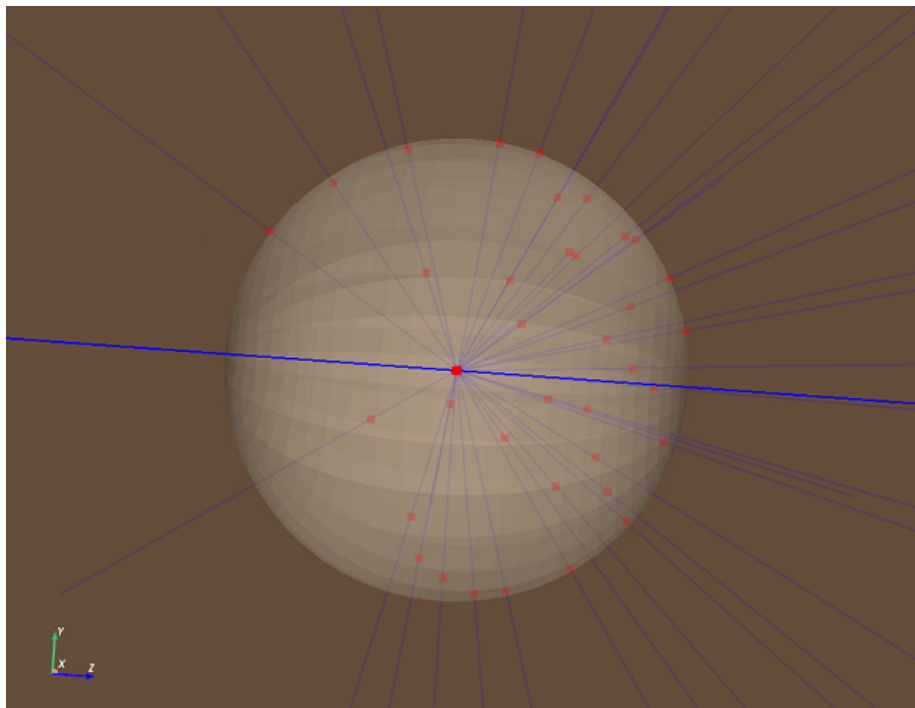


Figure 7: Geometry visualisation of the total scattering simulation

attached to the sample and used in cooperation with the detector to analyse the scattering number of a detected event.

A few `DeltaMomentum` scorers triggered by the `ENTRY PTS` are attached to the detector to obtain momentum transfer distribution of neutrons which are scattered at different times in the sample. Due to the special geometry of the detector, the accumulated single scattering $P(Q)$ is proportional to the static structure factor $S(Q)$. On the other hand, the employed CAB [DGM14] cross section for heavy water is generated in the Sköld approximation using Eq. 19. Hence the simulated structure factor is related to $S_{j,j'}(Q)$, the partial static structure factor, used in the cross section generation.

In Fig. 8, the single scattering momentum transfer distribution of the non-biased sample is compared with the interference differential scattering cross section (DCS) for heavy water measured by Soper [Sop13]. The structures of the simulated result are broadly similar to those in measurement. However, the widths of the peaks are slightly different. Also, the raising of the curve towards the lowest Q is not reproduced by the simulation. The observed discrepancies can be explained by the discrepancies between the static structure factor used in the cross section calculated and that from measurement.

As indicated by Eq. 19, the partial static structure factors should be used for polyatomic systems. To obtain that, the measured data need to be fitted to a microscopic model to determine the atomic structure candidate. Therefore, the peak width discrepancies are likely introduced by the fitting procedure. Secondly, the raising of the experimental data at low Q is caused by the liquid density fluctuation, which may not be included in the fitting model, hence not included in the cross section.

Fig. 9 shows the comparison of momentum transfer distribution $P(Q)$ of neutrons with different scattering numbers obtained from non-biased and biased runs. When Q is less than 3 \AA^{-1} , $P(Q)$ for all scatterings and single scattering are almost not distinguishable. However, the discrepancies between them grow with a greater Q value, suggesting that multiple scattering becomes more and more significant.

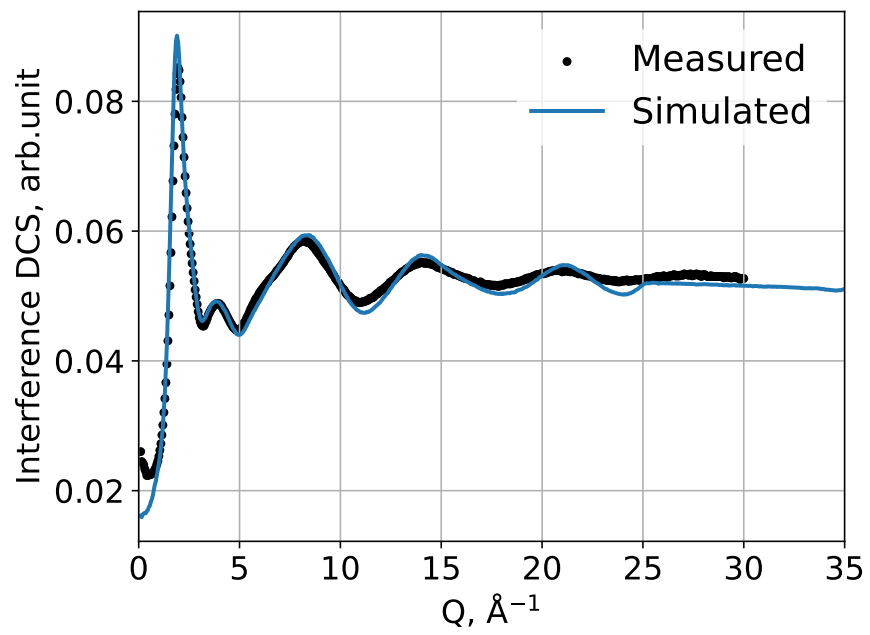


Figure 8: Comparisons between normalisation of the simulation result of Prompt and the measurements from Soper [Sop13]

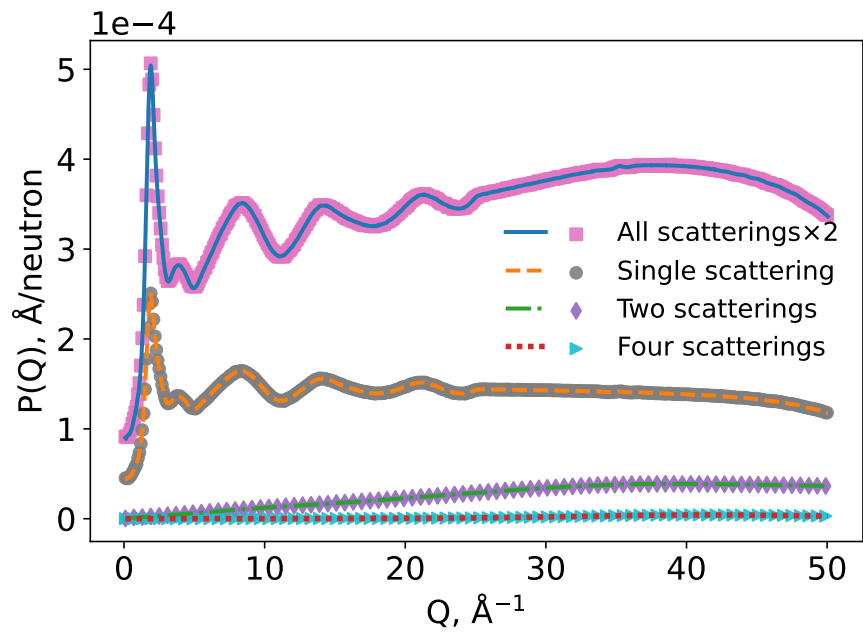


Figure 9: Comparisons between $P(Q)$ for different scattering numbers obtained from non-biased and biased runs. The solid, dashed, dash-dotted and dotted lines are respectively the results of all scatterings, single scattering, two scatterings and four scatterings from the non-biased run, while the squares, circles, diamonds, and triangles right are results of the biased run.

The results of two runs for the same scattering number are overlapped, hence the probability is conserved when the cross section biasing technique is applied. Although the number of incident neutrons of the biased run is only 10% of that of the non-biased run, their results are almost statistically equivalent. Therefore, the cross section biasing technique is able to improve the computational efficiency significantly.

4.2. Powder diffraction

A powder neutron diffraction example is simulated in `Prompt`, using the experiment configurations from PUS at the JEEP II Reactor in Norway [HFS+00]. Fig. 10 shows the visualisation of the geometry and 100 neutron trajectories.

In this example, a `UniModerator` particle gun is used for the moderator, with the widths and heights of 40 mm for both moderator and slit, the moderator is 1.9 m away from the downstream slit. Neutrons are uniformly distributed in a 0.05 Å interval and the mean wavelength is 1.54 Å. A 15' α_1 Soller collimator system is located downstream of the moderator, and composed of 22 pieces of B_4C blades. A single bent monochromator that contains nine Ge-511 single crystals is modelled as a single slab geometry. Such simplification neglects the focusing effects offered by the monochromator. It may have a large impact on the flux on sample and slightly change the instrument resolution function. In the simulation, a 54 mm × 116 mm × 8 mm single crystal germanium with 16' mosaicity is placed at the origin. Its front surface is parallel with the 511 reflection planes. The nominal glancing angle of the incident neutron is 45°. In the experiment, the mean wavelength of the monochromatic neutron is 1.5449 Å [HFS+00]. To match that, the lattice length of the original `NCrystal Ge_sg227.ncmat` file is adjusted accordingly to be 5.7131 Å. Downstream of the monochromator, a 1015 mm long trapezoid beam channel is embedded in the shielding wall and acts as the α_2 collimator of the instrument. Its effective divergent is 1.41°. The sample is placed 2.75 m away from the monochromator along the negative y axis. To skip the detector calibration procedures as those in typical experiments, a spherical 4π detector is used to cover all solid angles

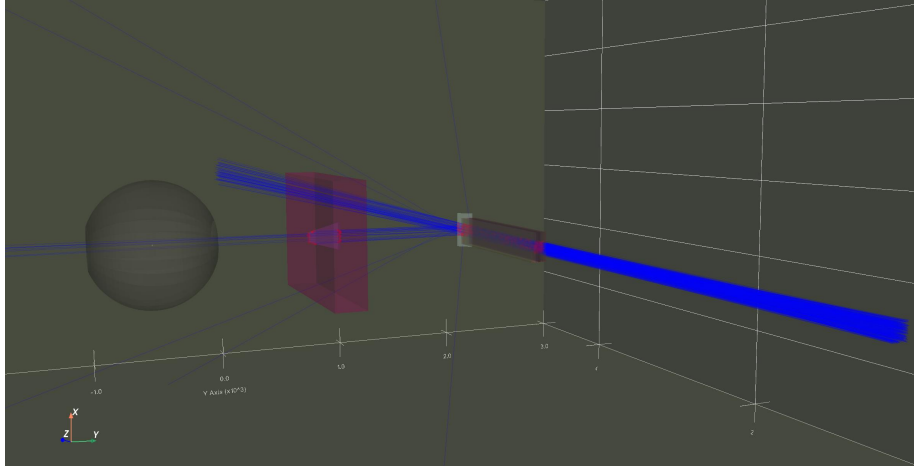


Figure 10: Visualisation of the simulated PUS instrument

in between 20° and 160° take-off angles. To eliminate any anisotropic effects, the sample is also made spherical with a 2.5 mm radius.

Fig. 11 shows the simulated powder diffraction pattern for the Al_2O_3 sample. The simulated and measured data are normalised by aligning the 143 peak at 124.1° . The intensity and resolution behaviours of the pattern are well captured by the simulation, and the observed agreements are very good. However, the experimental data is rising towards zero degrees. Similar behaviour is not observed in the simulation. In the experiments, the scattering environment between the sample and the detector is filled with helium; while in the simplified simulation, the environment is effectively vacuum. Likely, this discrepancy is introduced by the fact that the scattering in the gas is not modelled.

4.3. Neutron guide

The `Test_Guides.instr` setup in the McStas optical examples is reproduced in `Prompt`. The simulation world contains two position sensitive detectors and a guide. Fig. 12 shows the visualisation of the geometry and 100 neutron trajectories.

A front position sensitive detector, i.e. vacuum box attached by a `PSD ENTRY` type scorer, is placed 1 m away from the $50\text{ mm} \times 50\text{ mm}$ moderator surface that

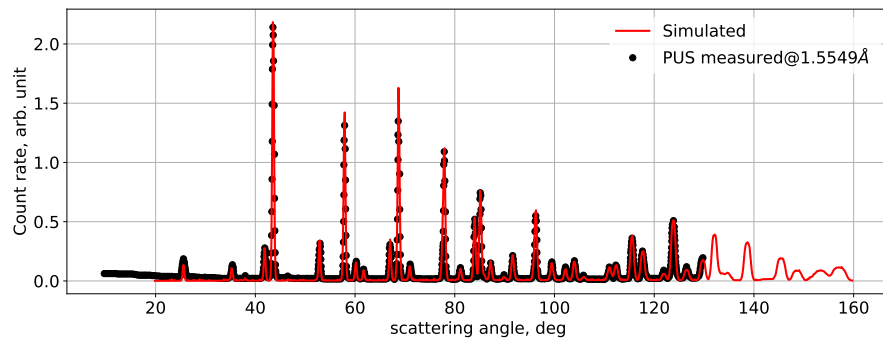


Figure 11: Simulated Al_2O_3 powder diffraction pattern at PUS

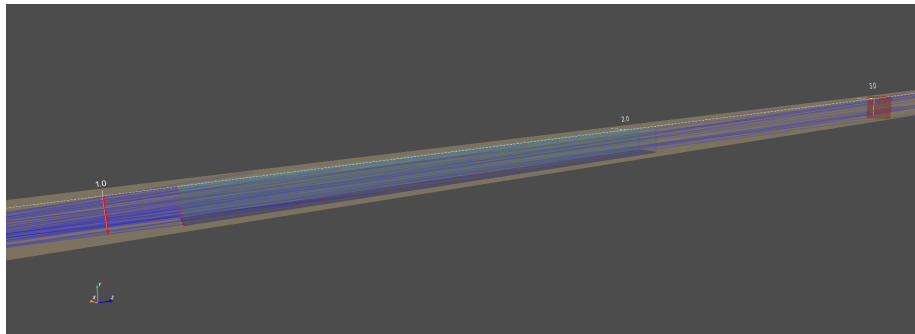


Figure 12: Geometry visualisation of the guide simulation

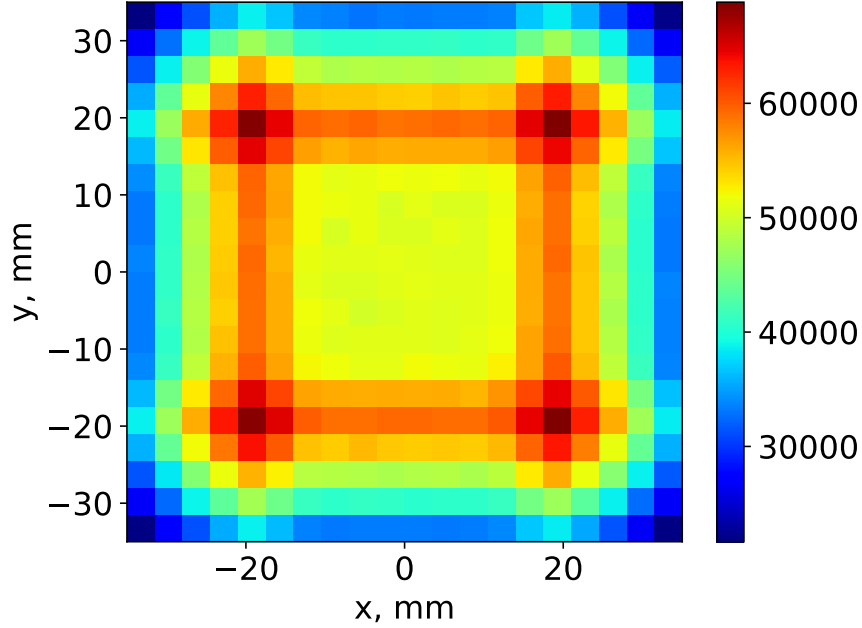


Figure 13: Rear position sensitive detector pattern

is emitting 3.39 \AA neutrons. Four boxes are used to form an $m = 1$ straight guide of which the inner opening is a $50 \text{ mm} \times 50 \text{ mm} \times 1000 \text{ mm}$ box. The entrance of the guide is 100 mm after the front detector. In addition, a rear position sensitive detector is placed 3.2 m away from the source along the line.

In the benchmark, 10^8 neutrons are simulated in about 140 s using a mid-2021 mainstream laptop. As the m value is too low to perfectly reflect such a divergent monochromatic beam, only about 19.34% of the neutrons reach the rear detector. The pattern on the detector is shown in Fig. 13. The square shape of the guide is visible and the four corners are highly distinguishable. The pattern from the McStas simulation of the same detector appears to be identical to that from Prompt, hence is not shown.

The integral intensity of the rear detector, normalised by the front detector count, is compared with that from McStas. Not surprisingly, as the reflectivity models are identical, the curves from these two packages are overlapped.

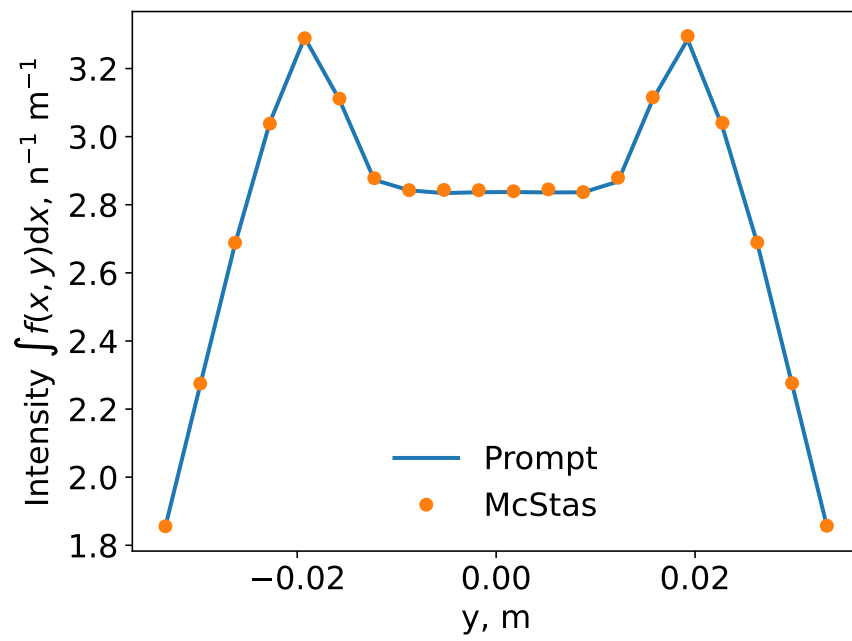


Figure 14: Comparison between the integral weight simulated by Prompt and that from McStas

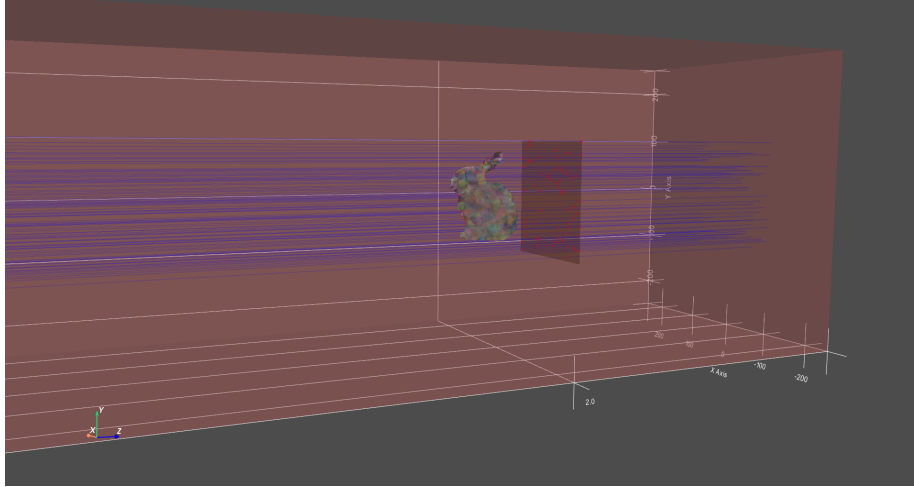


Figure 15: Visualization of simulation mission concerning the neutron imaging of Stanford bunny. 100 neutrons are shown for clarity

However, it is notable that McStas takes about half of the time to complete the simulation. Likely, the geometry module, i.e. VecGeom, in `Prompt` is not as effective as the ray-tracing algorithm used in McStas. On the other hand, `Prompt` is capable of modeling complex geometries as discussed in section 4.4.

4.4. Stanford bunny

A Stanford bunny [TL94] is simulated using `Prompt` in an imaging setup. The geometry visualisation is shown in Fig. 15. The bunny is in a surface mesh format originally, and the TetGen [Han15] code is used to generate a tetrahedral mesh of 2441 solids in total. In the simulation, the bunny is made of vanadium and approximately 15 cm in height. The bunny is irradiated in a parallel monochromatic 2 \AA neutrons beam. The beam size is $0.2 \text{ m} \times 0.2 \text{ m}$. Behind the bunny, an `ENTRY` type position detector is set up to measure the transmission pattern.

Two simulations are performed with two different absorption biases, 1 and 0.1. The images recorded by the detector are shown in Fig. 16. In both Fig. 16a and Fig. 16c, the shape of the object can be clearly observed. The biased simulation produces visibly identical results as the unbiased case.

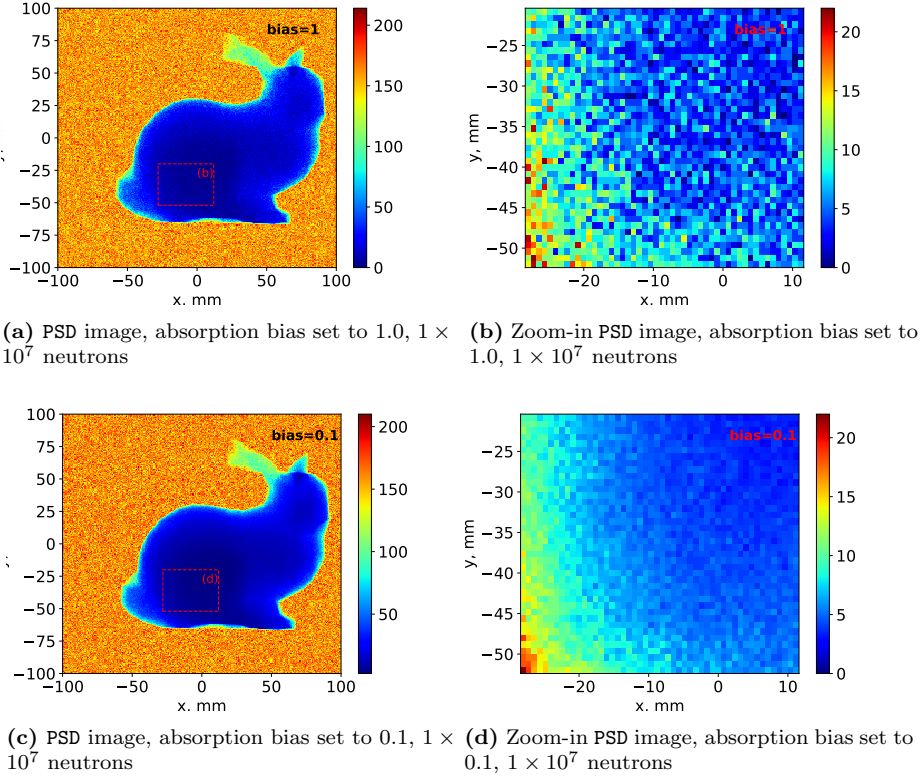


Figure 16: Images recorded from the PSD `scorer` and their zoom-in images. The absorption biases are set to 1 and 0.1, respectively. The images with 0.1 absorption bias looks 'smoother'

To compare the statistical uncertainties in these two simulations, the areas included in the rectangle of Fig. 16a and Fig. 16c are then zoomed-in to Fig. 16b and Fig. 16d, respectively. Evidently, there are much less fluctuation for the simulation where the absorption bias is set to 0.1 (Fig. 16c and Fig. 16d) than that with bias 1 (Fig. 16a and Fig. 16b), indicating that the cross section biasing mechanism shows its capability in variance reduction in this example.

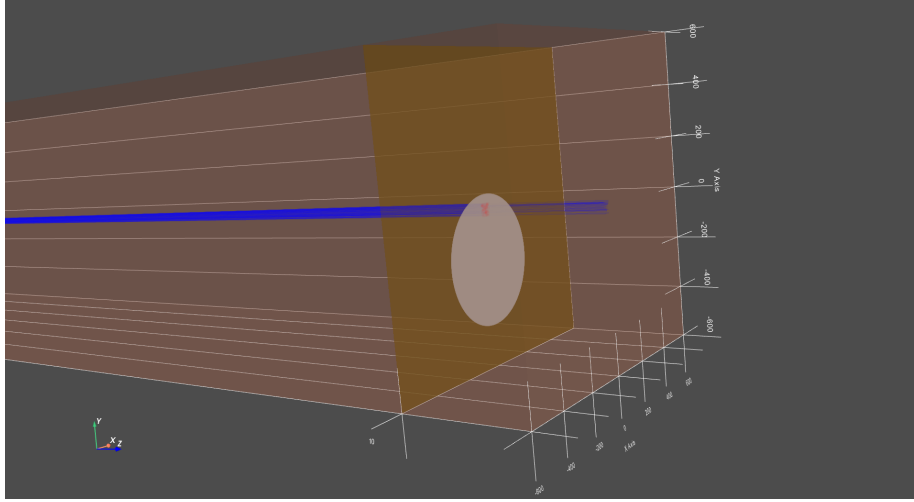


Figure 17: Visualization of DiskChopper simulation in Prompt, with 100 neutrons

4.5. Chopper

A simulation example of disk chopper is presented where the results are benchmarked with McStas, to demonstrate the ability of Prompt in neutron optical component simulation.

The simulation is visualised in Fig. 17. A disc-shaped (tube of negligible thickness) chopper with 4 axisymmetrically arranged 20° windows, of which the outer radius and inner radius are respectively 0.25 m and 0.13 m and the rotation frequency is 100 Hz, is located at 10 m away from a MaxwellianGun, which produces 293 K Maxwellian distributed neutrons from a $1\text{ mm} \times 1\text{ mm}$ opening to another 10 m away $45\text{ mm} \times 45\text{ mm}$ opening. The identical setup is reproduced in McStas as well to benchmark the implementation in Prompt. A time-of-flight scorer is positioned just behind and after the chopper to measure the impact of the chopper on the beam.

The time-of-flight spectra are compared in Fig. 18. Prompt produced the identical pattern as that from McStas. Eight peaks are evenly distributed in the time axis with 25 ms spacing. That is consistent with the 400 Hz frequency that the neutron beam sees the opening window.

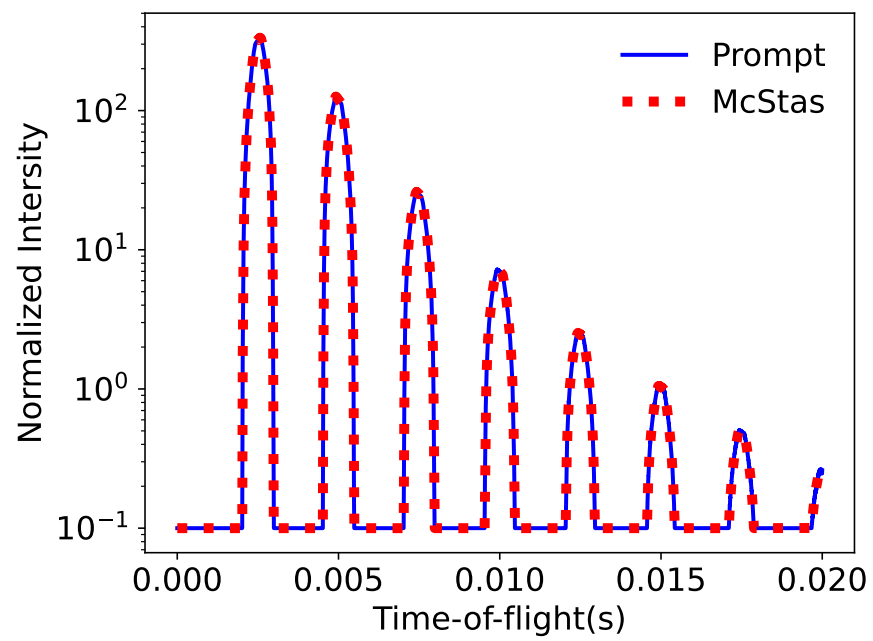


Figure 18: Benchmarking DiskChopper of Prompt with Diskchopper of McStas

5. Outlook

A thermal neutron simulation system is presented. As a standalone system, it is expected to be applicable in the areas of neutron instrument characterisation, optimisation as well as data analysis.

This system is the Monte Carlo module of the China Spallation Neutron Source Simulation System (**Cinema**). Two associated cross section calculation modules, Trajectory Analysis Toolkit(Tak) [DC22] and PiXiu, are currently under active development. They are essentially the post-analysis modules for molecular dynamics and density functional theory calculations, respectively. It is expected that the overall system should provide a full tool-chain to predict data that are directly comparable with instrument detector raw data from sample atomic structures and potentials. In parallel with **Cinema**, a machine learning framework is currently in the conceptual design phase. As the simulation tool-chain can describe the instruments and samples as parameters, the initial aim of this framework is for the optimisation of these parameters. To cope with this framework, **Prompt** is expected to become purely pythonic at the very top level shortly. It could be implemented as a python **GDML** manipulator or a direct interface to the **VecGeom** code. In any case, the system will be backward compatibility with the **GDML** user input introduced in this paper.

As an open source software project, it is straightforward to expand the system to cover more applications. Therefore, the future development of **Prompt** depends highly on community interest. For instance, a boundary overlap testing logic may be required for simulations with more complex geometries; supporting more particle types and physics models can enable the designs of moderators and shielding. The release of this system opens up many possibilities, feedback and inputs are welcome.

Acknowledgements

This research is supported by the National Natural Science Foundation of China (Grant No. 12075266) and the National Key Research and Development Program of China (Grant No. 2022YFA1604100). The authors are grateful for valuable discussions and substantial support.

References

- [A⁺05] G Amadio et al. GeantV: results from the prototype of concurrent vector particle transport simulation in HEP (2020), 2005.
- [ASL⁺12] D. L. Abernathy, M. B. Stone, M. J. Loguillo, M. S. Lucas, O. Delaire, X. Tang, J. Y. Y. Lin, and B. Fultz. Design and operation of the wide angular-range chopper spectrometer ARCS at the Spallation Neutron Source. Review of Scientific Instruments, 83(1):015114, 2012.
- [Ber17] Mads Bertelsen. Software for simulation and design of neutron scattering instrumentation. PhD thesis, University of Copenhagen, Faculty of Science, Niels Bohr Institute, Nano . . . , 2017.
- [CK20a] X.-X. Cai and T. Kittelmann. NCrystal: A library for thermal neutron transport. Computer Physics Communications, 246:106851, 2020.
- [CK20b] X.-X. Cai and T. Kittelmann. Ncrystal: A library for thermal neutron transport. Computer Physics Communications, 246:106851, 2020.
- [CKKM19] X.-X. Cai, T. Kittelmann, E. Klinkby, and J.I. Márquez Damián. Rejection-based sampling of inelastic neutron scattering. Journal of Computational Physics, 380:400–407, 2019.

- [CKL⁺18] Jie Chen, Le Kang, Huaile Lu, Ping Luo, Fangwei Wang, and Lunhua He. The general purpose powder diffractometer at CSNS. Physica B: Condensed Matter, 551:370–372, 2018. The 11th International Conference on Neutron Scattering (ICNS 2017).
- [CMPS06] Radovan Chytrcek, Jeremy McCormick, Witold Pokorski, and Giovanni Santin. Geometry description markup language for physics simulation and analysis applications. IEEE Transactions on Nuclear Science, 53(5):2892–2896, 2006.
- [Cre13] Jay Theodore Cremer. Small Angle Scatter with Correlation, Scatter and Intermediate Functions. In Advances in Imaging and Electron Physics, volume 175, pages 1–111. Elsevier, 2013.
- [DC22] Rong Du and X.-X. Cai. Convolutional discrete Fourier transform method for calculating thermal neutron cross section in liquids. Journal of Computational Physics, 466:111382, 2022.
- [DGM14] J.I. Márquez Damián, J.R. Granada, and D.C. Malaspina. CAB models for water: A new evaluation of the thermal neutron scattering laws for light and heavy water in ENDF-6 format. Annals of Nuclear Energy, 65:280–289, 2014.
- [DSTH99] L. L. Daemen, P. A. Seeger, T. G. Thelliez, and R. P. Hjelm. A Monte Carlo tool for simulations of neutron scattering instruments. AIP Conference Proceedings, 479(1):41–46, 1999.
- [EPN⁺11] G. Ehlers, A. A. Podlesnyak, J. L. Niedziela, E. B. Iverson, and P. E. Sokol. The new cold neutron chopper spectrometer at the Spallation Neutron Source: Design and performance. Review of Scientific Instruments, 82(8):085108, 2011.
- [gdm22] GDML USER’S GUIDE. <https://gdml.web.cern.ch/GDML/doc/GDMLmanual.pdf>, 2022. [Last modified 06/10/2022].

- [Han15] Si Hang. TetGen, a Delaunay-based quality tetrahedral mesh generator. ACM Trans. Math. Softw, 41(2):11, 2015.
- [HFS⁺00] Bjørn C. Hauback, Helmer Fjellvåg, Olav Steinsvoll, Kjell Johansson, Ole Tore Buset, and Johnny Jørgensen. The high resolution Powder Neutron Diffractometer PUS at the JEEP II reactor at Kjeller in Norway. Journal of Neutron Research, 8(3):215–232, 2000.
- [HMvdWea20] C.R. Harris, K.J. Millman, S.J. van der Walt, and et al. Array programming with NumPy. Nature, 585:357–362, 2020.
- [KC21] T. Kittelmann and X.-X. Cai. Elastic neutron scattering models for NCrystal. Computer Physics Communications, 267:108082, 2021.
- [KC23] Thomas Kittelmann and Xiao-Xiao Cai. NCrystal wikipedia. <https://github.com/mctools/ncrystal/wiki>, 2023. Last accessed 1 Feb 2023.
- [KKK⁺17] T. Kittelmann, E. Klinkby, E.B. Knudsen, P. Willendrup, X.X. Cai, and K. Kanaki. Monte carlo particle lists: MCPL. Computer Physics Communications, 218:17–42, 2017.
- [KNI⁺11] Ryoichi Kajimoto, Mitsutaka Nakamura, Yasuhiro Inamura, Fumio Mizuno, Kenji Nakajima, Seiko Ohira-Kawamura, Tetsuya Yokoo, Takeshi Nakatani, Ryuji Maruyama, Kazuhiko Soyama, Kaoru Shibata, Kentaro Suzuya, Setsuo Sato, Kazuya Aizawa, Masatoshi Arai, Shuichi Wakimoto, Motoyuki Ishikado, Shinichi Shamoto, Masaki Fujita, Haruhiro Hiraka, Kenji Ohoyama, Kazuyoshi Yamada, and Chul-Ho Lee. The Fermi Chopper Spectrometer 4SEASONS at J-PARC. Journal of the Physical Society of Japan, 80(Suppl.B):SB025, 2011.

- [KYN⁺19] Ryoichi Kajimoto, Tetsuya Yokoo, Mitsutaka Nakamura, Yuki-nobu Kawakita, Masato Matsuura, Hitoshi Endo, Hideki Seto, Shinichi Itoh, Kenji Nakajima, and Seiko Ohira-Kawamura. Status of neutron spectrometers at J-PARC. Physica B: Condensed Matter, 562:148–154, 2019.
- [LBC⁺11] Mats Lindroos, S Bousson, R Calaga, Håkan Danared, G Devanz, R Duperrier, J Eguia, Mohammad Eshraqi, S Gammino, Håkan Hahn, et al. The European spallation source. Nuclear Instruments and Methods in Physics Research Section B: Beam Interactions with Materials and Atoms, 269(24):3258–3260, 2011.
- [LN99] Kim Lefmann and Kristian Nielsen. McStas, a general software package for neutron ray-tracing simulations. Neutron news, 10(3):20–23, 1999.
- [LNA⁺06] K. Lefmann, Ch. Niedermayer, A.B. Abrahamsen, C.R.H. Bahl, N.B. Christensen, H.S. Jacobsen, T.L. Larsen, P. Häfliger, U. Filges, and H.M. Rønnow. Realizing the full potential of a RITA spectrometer. Physica B: Condensed Matter, 385-386:1083–1085, 2006.
- [Lov84] S W Lovesey. Theory of neutron scattering from condensed matter. Vol. 1. Nuclear scattering. Oxford Science Publications, Jan 1984.
- [MAA⁺06] T.E. Mason, D. Abernathy, I. Anderson, J. Ankner, T. Egami, G. Ehlers, A. Ekkebus, G. Granroth, M. Hagen, K. Herwig, J. Hodges, C. Hoffmann, C. Horak, L. Horton, F. Klose, J. Larese, A. Mesezar, D. Myles, J. Neufeind, M. Ohl, C. Tulk, X-L. Wang, and J. Zhao. The Spallation Neutron Source in Oak Ridge: A powerful tool for materials research. Physica B: Condensed Matter, 385-386:955–960, 2006.

- [MK10] R. MacFarlane and A. Kahler. Methods for processing ENDF/B-VII with NJOY. Nucl. Data Sheets, 111(12):2739–2890, 2010.
- [MW12] Marcus H. Mendenhall and Robert A. Weller. A probability-conserving cross-section biasing mechanism for variance reduction in Monte Carlo particle transport calculations. Nuclear Instruments and Methods in Physics Research Section A: Accelerators, Spectrometers, Detectors and Associated Equipment, 667:38–43, 2012.
- [OMR⁺04] M Ohl, M Monkenbusch, D Richter, C Pappas, K Lieutenant, Th Krist, G Zsigmond, and F Mezei. The high-resolution neutron spin-echo spectrometer for the SNS with $\tau \geq 1 \mu\text{s}$. Physica B: Condensed Matter, 350(1-3):147–150, 2004.
- [RSS62] A. Rahman, K. S. Singwi, and A. Sjölander. Theory of Slow Neutron Scattering by Liquids. I. Phys. Rev., 126:986–996, May 1962.
- [Sch14] Helmut Schober. An Introduction to the Theory of Nuclear Neutron Scattering in Condensed Matter. Journal of Neutron Research, 17(3-4):109 – 357, 2014.
- [SD04] Philip A Seeger and Luke L Daemen. The neutron instrument simulation package, NISP. In Advances in Computational Methods for X-Ray and Neutron Optics, volume 5536, pages 109–123. SPIE, 2004.
- [SDJE06] J. R. Santisteban, M. R. Daymond, J. A. James, and L. Edwards. ENGIN-X: a third-generation neutron strain scanner. Journal of Applied Crystallography, 39(6):812–825, Dec 2006.
- [Sjö58] Alf Sjölander. Multi-phonon processes in slow neutron scattering by crystals. Arkiv För fysik, 14(21):315–371, 1958.

- [ŠK97] J Šaroun and J Kulda. RESTRAX—a program for TAS resolution calculation and scan profile simulation. Physica B: Condensed Matter, 234:1102–1104, 1997.
- [SK04] Jan Saroun and Jiri Kulda. Neutron ray-tracing simulations and data analysis with RESTRAX. In Advances in Computational Methods for X-Ray and Neutron Optics, volume 5536, pages 124–133. SPIE, 2004.
- [Skö67] Kurt Sköld. Small Energy Transfer Scattering of Cold Neutrons from Liquid Argon. Phys. Rev. Lett., 19:1023–1025, Oct 1967.
- [Sop13] Alan K Soper. The radial distribution functions of water as derived from radiation total scattering experiments: Is there anything we can say for sure? International Scholarly Research Notices, 2013, 2013.
- [Squ12] G. L. Squires. Introduction to the Theory of Thermal Neutron Scattering. Cambridge University Press, 3 ed. edition, 2012.
- [SSP95] Varley F. Sears, Eric C. Svensson, and Brian M. Powell. Phonon density of states in vanadium. Canadian Journal of Physics, 73:726–734, 1995.
- [Tay06] Andrew Taylor. PROGRESS at the ISIS Facility. Physica B: Condensed Matter, 385-386:728–731, 2006.
- [TL94] Greg Turk and Marc Levoy. Zippered polygon meshes from range images. In Proceedings of the 21st annual conference on Computer graphics and interactive techniques, pages 311–318, 1994.
- [VH54] Léon Van Hove. Correlations in Space and Time and Born Approximation Scattering in Systems of Interacting Particles. Phys. Rev., 95:249–262, Jul 1954.

- [WCC⁺09] Jie Wei, Hesheng Chen, Yanwei Chen, Yuanbo Chen, Yunlong Chi, Changdong Deng, Haiyi Dong, Lan Dong, Shouxian Fang, Ji Feng, et al. China spallation neutron source: design, R&D, and outlook. Nuclear Instruments and Methods in Physics Research Section A: Accelerators, Spectrometers, Detectors and Associated Equipment, 600(1):10–13, 2009.
- [WFK⁺22] P. Willendrup, E. Farhi, E. Knudsen, U. Filges, and K. Lefmann. Component Manual for the Neutron Ray-Tracing Package McStas, version 2.7.2. <https://www.mcstas.org/download/components/2.7.2/doc/manuals/mcstas-components.pdf>, December 2022.
- [WL20] Peter Kjær Willendrup and Kim Lefmann. McStas (i): Introduction, use, and basic principles for ray-tracing simulations. Journal of Neutron Research, 22:1–16, 2020.
- [ZLM02] G Zsigmond, K Lieutenant, and F Mezei. Monte Carlo simulations of neutron scattering instruments by VITESS: Virtual instrumentation tool for ESS. Neutron News, 13(4):11–14, 2002.
- [ZLM⁺04] G Zsigmond, K Lieutenant, S Manoshin, HN Bordallo, JDM Champion, J Peters, JM Carpenter, and F Mezei. A survey of simulations of complex neutronic systems by VITESS. Nuclear Instruments and Methods in Physics Research Section A: Accelerators, Spectrometers, Detectors and Associated Equipment, 529(1-3):218–222, 2004.

Appendix A. Supported solids

Appendix A.1. Arbitrary_trapezoid

Listing A.1: An example: definition of an arbitrary_trapezoid

```
<arb8 lunit="mm" name="Arb8Solid" v1x="-30" v1y="-60" v2x="30" ↵  
↵v2y="-60" v3x="50" v3y="60" v4x="-50" v4y="60" v5x="-30" v5y="-  
↵60" v6x="30" v6y="-60" v7x="50" v7y="60" v8x="-50" v8y="60" dz=  
↵"70"/>
```

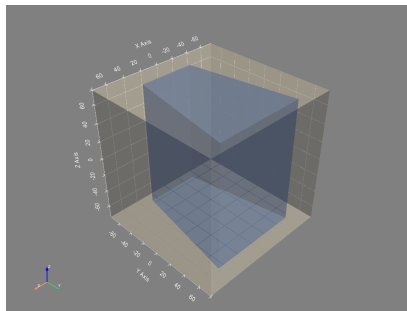


Figure A.1: Visualization of an arbitrary_trapezoid

Table A.1: Parameters for defining an arbitrary_trapezoid. If not specified, default length unit is *mm*

Parameter	Description
v1x	vertex 1 x position
v1y	vertex 1 y position
v2x	vertex 2 x position
v2y	vertex 2 y position
v3x	vertex 3 x position
v3y	vertex 3 y position
v4x	vertex 4 x position
v4y	vertex 4 y position
v5x	vertex 5 x position
v5y	vertex 5 y position
v6x	vertex 6 x position
v6y	vertex 6 y position
v7x	vertex 7 x position
v7y	vertex 7 y position
v8x	vertex 8 x position
v8y	vertex 8 y position
dz	half z length

Appendix A.2. Box

Listing A.2: An example: definition of a box. If not specified, default length unit is *mm*

```
<box lunit="mm" name="BoxSolid" x="100.0" y="100.0" z="100.0"/>
```

Table A.2: Parameters for defining a box. If not specified, default length unit is *mm*

Parameter	Description
x	half length in x direction
y	half length in y direction
z	half length in z direction

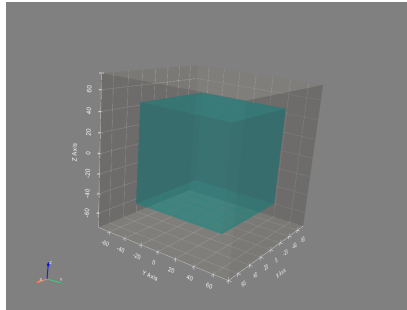


Figure A.2: Visualization of a box

Appendix A.3. Cone

Listing A.3: An example: definition of a cone

```
<cone aunit="deg" lunit="mm" name="ConeSolid" rmin1="0.0" rmax1=  
→"50.0" rmin2="0.0" rmax2="10.0" z="120.0" deltaphi="360.0" ↵  
→startphi="0.0" />
```

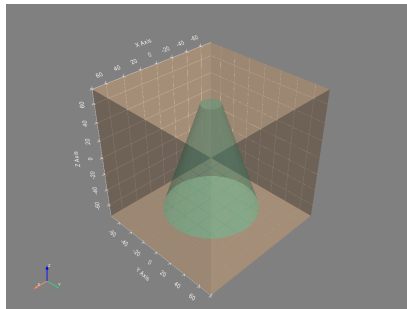


Figure A.3: Visualization of a cone

Table A.3: Parameters for defining a cone. If not specified, default length unit is *mm*, default angle unit is *deg*

Parameter	Description
<code>rmin1</code>	inner radius at base of cone
<code>rmax1</code>	outer radius at base of cone
<code>rmin2</code>	inner radius at top of cone
<code>rmax2</code>	outer radius at top of cone
<code>z</code>	height of cone segment
<code>startphi</code>	start angle of the segment
<code>deltaphi</code>	angle of the segment

Appendix A.4. CutTube

Listing A.4: An example: definition of a cutTube

```
<cutTube aunit="deg" lunit="mm" name="CutTubeSolid" rmin="10.0"
→rmax="25.0" z="50.0" deltaphi="360.0" startphi="0.0" lowX="-5"
→lowY="-5" lowZ="-5" highX="5" highY="5" highZ="5"/>
```

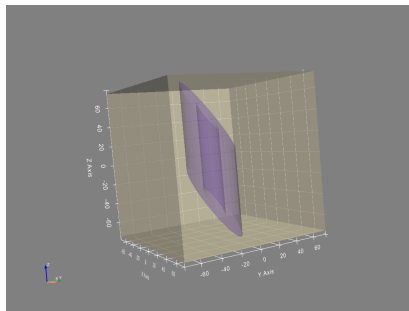


Figure A.4: Visualization of a cutTube

Table A.4: Parameters for defining a cutTube. If not specified, default length unit is *mm*, default angle unit is *deg*

Parameter	Default	Description
<code>z</code>		length along z axis
<code>rmin</code>	0.0	inner radius
<code>rmax</code>		outer radius
<code>startphi</code>	0.0	starting phi angle of segment
<code>deltaphi</code>		delta phi of angle
<code>lowX</code>		normal at lower z plane
<code>lowY</code>		normal at lower z plane
<code>lowZ</code>		normal at lower z plane
<code>highX</code>		normal at upper z plane
<code>highY</code>		normal at upper z plane
<code>highZ</code>		normal at upper z plane

Appendix A.5. General_trapezoid

Listing A.5: An example: definition of a general_trapezoid

```
<trap lunit="mm" name="TrapSolid" z="130" thata="45" phi="45" y1=
↪"60" x1="40" x2="40" alpha1="45" y2="60" x3="40" x4="40" ↪
↪alpha2="45"/>
```

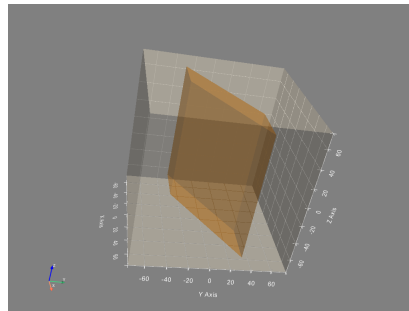


Figure A.5: Visualization of a general_trapezoid

Table A.5: Parameters for defining a general_trapezoid. If not specified, default length unit is *mm*

Parameter	Description
z	length along z axis
theta	polar angle to faces joining at -/+z
phi	azimuthal angle of line joining centre of -z face to centre of +z face
y1	length along y at the face -z
x1	length along x at side y = -y1 of the face at -z
x2	length along x at side y = +y1 of the face at -z
alpha1	angle with respect to the y axis from the centre of side at y = -y1 to centre of y = +y1 of the face at -z
y2	length along y at the face +z
x3	length along x at side y = -y1 of the face at +z
x4	length along x at side y = +y1 of the face at +z
alpha2	angle with respect to the y axis from the centre of side at y = -y2 to centre of y = +y2 of the face at +z

Appendix A.6. Hyperbolic_tube

Listing A.6: An example: definition of a hyperbolic_tube

```
<hype lunit="mm" name="HypeSolid" rmin="10" rmax="20" z="100"
  ↪inst="0.785" outst="0.785"/>
```

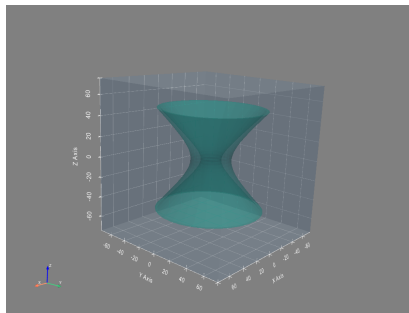


Figure A.6: Visualization of a hyperbolic_tube

Table A.6: Parameters for defining a `hyperbolic_tube`. If not specified, default length unit is *mm*. Stereo angle unit can only be *rad*

Parameter	Description
<code>rmin</code>	inside radius of tube
<code>rmax</code>	outside radius of tube
<code>inst</code>	inner stereo
<code>outst</code>	outer stereo
<code>z</code>	z length

Appendix A.7. Orb

Listing A.7: An example: definition of an orb

```
<orb lunit="mm" name="OrbSolid" r="50"/>
```

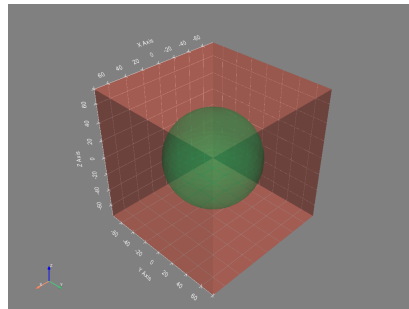


Figure A.7: Visualization of an orb

Table A.7: Parameters for defining an orb. If not specified, default length unit is *mm*

Parameter	Description
<code>r</code>	radius

Appendix A.8. Paraboloid

Listing A.8: An example: definition of a paraboloid

```
<paraboloid lunit="mm" name="ParaboloidSolid" rlo="60.0" rhi="10.  
↪0" dz="60.0"/>
```

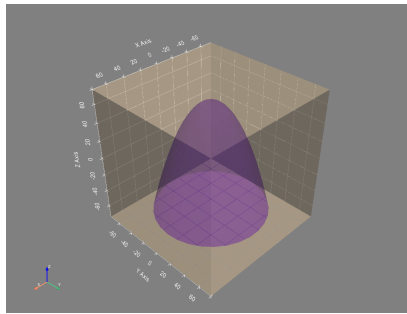


Figure A.8: Visualization of a paraboloid

Table A.8: Parameters for defining a paraboloid. If not specified, default length unit is *mm*

Parameter	Description
rlo	radius at $-z$
rhi	radius at $+z$
dz	z length

Appendix A.9. Polycone

Listing A.9: An example: definition of a polycone

```
<polycone aunit="deg" lunit="mm" name="PolyconeSolid" deltaphi=  
↪"360.0" startphi="0.0">  
  <zplane rmin="10.0" rmax="20.0" z="60.0"/>  
  <zplane rmin="30.0" rmax="50.0" z="-50.0" />  
</polycone>
```

Table A.9: Parameters for defining a polycone. If not specified, default length unit is *mm*, default angle unit is *deg*

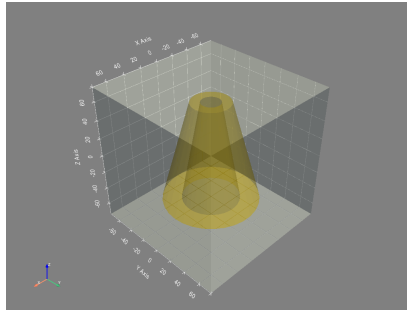


Figure A.9: Visualization of a polycone

Parameter	Default	Sub-parameter and description	
<code>startphi</code>	0.0		start angle of the segment
<code>deltaphi</code>			angle of the segment
<code>zplane</code>	0.0	<code>rmin</code>	inner radius of cone at this point
		<code>rmax</code>	outer radius of cone at this point
		<code>z</code>	z coordinate of the plane

Appendix A.10. Polyhedra

Listing A.10: An example: definition of a polyhedra

```
<polyhedra aunit="deg" lunit="mm" name="PolyhedraSolid" deltaphi=
→"360.0" startphi="0.0" numsides="6">
  <zplane rmin="20.0" rmax="50.0" z="-50.0"/>
  <zplane rmin="5.0" rmax="10.0" z="0.0" />
  <zplane rmin="10.0" rmax="30.0" z="60.0" />
</polyhedra>
```

Table A.10: Parameters for defining a polyhedra. If not specified, default length unit is *mm*, default angle unit is *deg*

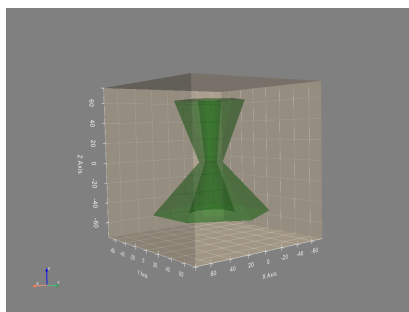


Figure A.10: Visualization of a polyhedra

Parameter	Default	Sub-parameter and description	
<code>startphi</code>		start angle of the segment	
<code>deltaphi</code>		angle of the segment	
<code>numsides</code>		number of sides	
<code>zplane</code>	0.0	<code>rmin</code>	inner radius of cone at this point
		<code>rmax</code>	outer radius of cone at this point
		<code>z</code>	z coordinate of the plane

Appendix A.11. Sphere

Listing A.11: An example: definition of a sphere

```
<sphere aunit="deg" lunit="mm" name="SphereSolid" rmin="0.0"
→rmax="60.0" deltaphi="180.0" startphi="0.0" deltatheta="90.0"
→starttheta="0.0"/>
```

Table A.11: Parameters for defining a sphere. If not specified, default length unit is *mm*, default angle unit is *deg*

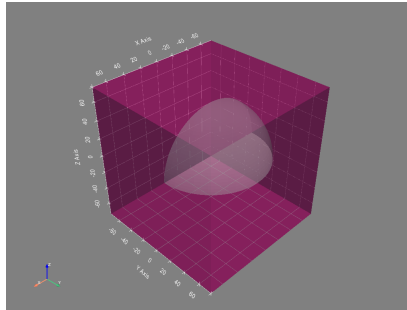


Figure A.11: Visualization of a sphere

Parameter	Default	Description
<code>rmin</code>	0.0	inner radius
<code>rmax</code>		outer radius
<code>startphi</code>	0.0	starting angle of the segment
<code>deltaphi</code>		delta angle of the segment
<code>starttheta</code>	0.0	starting angle of the segment
<code>deltatheta</code>		delta angle of the segment

Appendix A.12. Tetrahedron

Listing A.12: An example: definition of a tetrahedron

```

<define>
  <position name="v1" x="-70" y="-70" z="-60"/>
  <position name="v2" x="70" y="-40" z="-60"/>
  <position name="v3" x="0" y="60" z="-60"/>
  <position name="v4" x="0" y="0" z="60"/>
</define>
<tet name="TetrahedronSolid" vertex1="v1" vertex2="v2" vertex3=
→"v3" vertex4="v4"/>

```

Table A.12: Parameters for defining a tetrahedron. If not specified, default length unit is *mm*

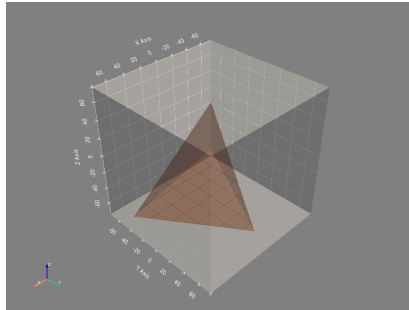


Figure A.12: Visualization of a tetrahedron

Parameter	Description
vertex1	vertex 1 position
vertex2	vertex 2 position
vertex3	vertex 3 position
vertex4	vertex 4 position

Appendix A.13. Trapezoid

Listing A.13: An example: definition of a trapezoid

```
<trd lunit="mm" name="TrdSolid" x1="50" x2="100" y1="60" y2="80"
  ↪ " z="130"/>
```

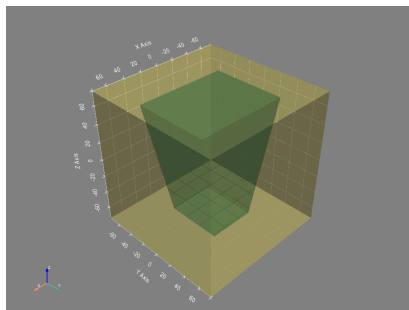


Figure A.13: Visualization of a trapezoid

Table A.13: Parameters for defining a trapezoid. If not specified, default length unit is *mm*

Parameter	Description
x1	x length at -z
x2	x length at +z
y1	y length at -z
y2	y length at +z
z	z length

Appendix A.14. Tube

Listing A.14: An example: definition of a tube

```
<tube aunit="deg" lunit="mm" name="TubeSolid" rmin="10.0" rmax=
↪"50.0" z="120.0" deltaphi="360.0" startphi="0.0"/>
```

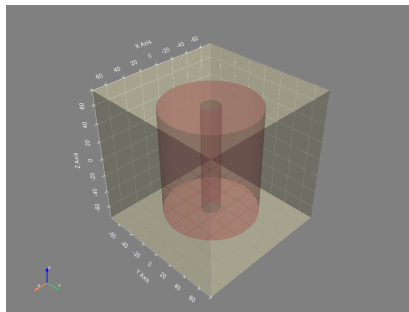


Figure A.14: Visualization of a tube

Table A.14: Parameters for defining a tube. If not specified, default length unit is *mm*, default angle unit is *deg*

Parameter	Default	Description
<code>rmin</code>	0.0	inside radius of segment
<code>rmax</code>		outside radius of segment
<code>z</code>		z length of tube segment
<code>startphi</code>	0.0	starting phi position angle of segment
<code>deltaphi</code>		delta angle of segment

Appendix B. Particle guns

Appendix B.1. SimpleThermalGun

Table B.1: Parameters available in `SimpleThermalGun` configuration strings. Parameters without default values are required, the others are optional.

Parameter	Default	Description	Unit
<code>energy</code>	0	Energy of particles. The value can be positive ¹ or zero ²	eV
<code>position</code>		Position of primary particles.	mm
<code>direction</code>	0,0,1	Direction vector of primary particles.	mm

¹ Single energy of input value.

² Maxwell's distribution with temperature of 293 K.

Appendix B.2. IsotropicGun

Table B.2: Parameters available in `IsotropicGun` configuration strings. Parameters without default values are required, the others are optional.

Parameter	Default	Description	Unit
<code>energy</code>	0	Energy of particles. The value can be positive ¹ or zero ²	eV
<code>position</code>		Position of primary particles.	mm

¹ Single energy of input value.

² Maxwell's distribution with temperature of 293 K.

Appendix B.3. UniModeratorGun

Table B.3: Parameters available in `UniModeratorGun` configuration strings. Parameters without default values are required, the others are optional.

Parameter	Default	Description	Unit
<code>src_w</code>		X-dimension (width) of particle source surface.	mm
<code>src_h</code>		Y-dimension (height) of particle source surface.	mm
<code>src_z</code>		Z-coordinate of particle source center in global reference system.	mm
<code>slit_w</code>		X-dimension (width) of slit surface.	mm
<code>slit_h</code>		Y-dimension (height) of slit surface.	mm
<code>slit_z</code>		Z-coordinate of slit center in global reference system.	mm
<code>mean_wl</code>	1	Mean wavelength of primary particles.	Å
<code>range_wl</code>	0.0001	The width of the uniform wavelength distribution.	Å

Appendix B.4. MaxwellianGun

Table B.4: Parameters available in `MaxwellianGun` configuration strings. Parameters without default values are required, the others are optional.

Parameter	Default	Description	Unit
<code>src_w</code>		X-dimension (width) of particle source surface.	mm
<code>src_h</code>		Y-dimension (height) of particle source surface.	mm
<code>src_z</code>		Z-coordinate of particle source center in global reference system.	mm
<code>slit_w</code>		X-dimension (width) of slit surface.	mm
<code>slit_h</code>		Y-dimension (height) of slit surface.	mm
<code>slit_z</code>		Z-coordinate of slit center in global reference system.	mm
<code>temperature</code>	293.15	Temperature of Maxwellian energy distribution.	K

Appendix B.5. MCPLGun

Table B.5: Parameters available in MCPLGun configuration strings. Parameters without default values are required, the others are optional.

Parameter	Default	Description	Unit
mcplfile		Input MCPL file.	str

Appendix C. Scorers

Appendix C.1. ESpectrum

Table C.1: Parameters available in ESpectrum configuration strings. Parameters without default values are required, the others are optional.

Parameter	Default	Description	Unit
name		Name of the histogram.	str
min		Minimum energy of the histogram.	eV
max		Maximum energy of the histogram.	eV
numbin	100	Bin number of the histogram.	1
ptstate	ENTRY	Particle tracing state, available options are: SURFACE, ENTRY, ABSORB, PROPAGATE, EXIT.	str

Appendix C.2. WLSpectrum

Table C.2: Parameters available in WLSpectrum configuration strings. Parameters without default values are required, the others are optional.

Parameter	Default	Description	Unit
name		Name of the histogram.	str
min		Minimum wavelength of the histogram.	Å
max		Maximum wavelength of the histogram.	Å
numbin	100	Bin number of the histogram.	1
ptstate	ENTRY	Particle tracing state, available options are: SURFACE, ENTRY, ABSORB, PROPAGATE, EXIT.	str

Appendix C.3. TOF

Table C.3: Parameters available in TOF configuration strings. Parameters without default values are required, the others are optional.

Parameter	Default	Description	Unit
<code>name</code>		Name of the histogram.	str
<code>min</code>		Minimum time of the histogram.	s
<code>max</code>		Maximum time of the histogram.	s
<code>numbin</code>	100	Bin number of the histogram.	1
<code>ptstate</code>	ENTRY	Particle tracing state, available options are: SURFACE, ENTRY, ABSORB, PROPAGATE, EXIT.	str

Appendix C.4. PSD

Table C.4: Parameters available in PSD configuration strings. Parameters without default values are required, the others are optional.

Parameter	Default	Description	Unit
<code>name</code>		Name of the histogram.	str
<code>xmin</code>		Minimum x of the histogram.	mm
<code>xmax</code>		Maximum x of the histogram.	mm
<code>numbin_x</code>	100	Bin number of X-axis.	1
<code>ymin</code>		Minimum y of the histogram.	mm
<code>ymax</code>		Maximum y of the histogram.	mm
<code>numbin_y</code>	100	Bin number of Y-axis.	1
<code>type</code>	XY	Projection plane of the volume, can be set to: XY ¹ , XZ or YZ.	str
<code>ptstate</code>	ENTRY	Particle tracing state, available options are: SURFACE, ENTRY, ABSORB, PROPAGATE, EXIT.	str

¹ For instance, XY implies the projection of the volume on XY-plane.

Appendix C.5. MultiScat

Table C.5: Parameters available in `MultiScat` configuration strings. Parameters without default values are required, the others are optional.

Parameter	Default	Description	Unit
<code>name</code>		Name of the histogram.	str
<code>min</code>	0	Minimum scattering number of the histogram.	1
<code>max</code>	5	Maximum scattering number of the histogram.	1
<code>linear</code>	yes	Linear option for X-axis of the histogram. ¹	str

¹ The default, `yes`, implies the linear X-axis, while `no` changes the X-axis to log scale.

Appendix C.6. DeltaMomentum

Table C.6: Parameters available in `DeltaMomentum` configuration strings. Parameters without default values are required, the others are optional.

Parameter	Default	Description	Unit
<code>name</code>		Name of the histogram.	str
<code>sample_pos</code>		Position vector of sample in global reference.	mm
<code>beam_dir</code>		Direction vector of beam.	mm
<code>dist</code>		Distance between neutron source and sample.	mm
<code>min</code>		Minimum Q of the histogram.	\AA^{-1}
<code>max</code>		Maximum Q of the histogram.	\AA^{-1}
<code>numbin</code>	100	Bin number of the histogram.	1
<code>method</code>	0	Method for calculating momentum transfer Q ¹	str
<code>ptstate</code>	ENTRY	Particle tracing state, available options are: SURFACE, ENTRY, ABSORB, PROPAGATE, EXIT.	str
<code>linear</code>	yes	Linear option for X-axis of the histogram ²	str
<code>scatnum</code>	-1	Scattering number to be counted ³	1

¹ The default value 0 implies momentum transfer of inelastic scattering, while a value of 1 means momentum transfer of elastic scattering.

² The default, **yes**, implies the linear X-axis, while **no** changes the X-axis to log scale.

³ Should be an integer greater than or equal to -1. The default value implies the histogram accumulates event regardless of the scattering number. Other values enables the accumulation on the specified scattering number. The scattering number is counted by a `MultiScat` scorer, hence such a scorer should be attached to the volume of interest if `scatnum` is other than -1.

Appendix C.7. Angular

Table C.7: Parameters available in `Angular` configuration strings. Parameters without default values are required, the others are optional.

Parameter	Default	Description	Unit
<code>name</code>		Name of the histogram.	str
<code>sample_pos</code>		Position vector of sample in global reference.	mm
<code>beam_dir</code>		Direction vector of beam.	mm
<code>dist</code>		Distance between particle source and sample.	mm
<code>min</code>		Minimum scattering angle of the histogram, range of which should be $[0, 180]^\circ$.	$^\circ$
<code>max</code>		Maximum scattering angle of the histogram, range of which should be $[0, 180]^\circ$.	$^\circ$
<code>numbin</code>	100	Bin number of the histogram.	1
<code>ptstate</code>	ENTRY	Particle tracing state, available options are: SURFACE, ENTRY, ABSORB, PROPAGATE, EXIT.	str
<code>linear</code>	yes	Linear option for X-axis of the histogram. ¹	str

¹ The default, `yes`, implies the linear X-axis, while `no` changes the X-axis to log scale.

Appendix C.8. VolFluence

Table C.8: Parameters available in VolFluence configuration strings. Parameters without default values are required, the others are optional.

Parameter	Default	Description	Unit
<code>name</code>		Name of the histogram.	str
<code>min</code>		Minimum energy of the histogram.	eV
<code>max</code>		Maximum energy of the histogram.	eV
<code>numbin</code>	100	Bin number of the histogram.	1
<code>ptstate</code>	PROPAGATE	Particle tracing state, available options are: SURFACE, ENTRY, ABSORB, PROPAGATE, EXIT.	str
<code>linear</code>	yes	Linear option for X-axis of the histogram. ¹	str

¹ The default, `yes`, implies the linear X-axis, while `no` changes the X-axis to log scale.